UT-ICEPP 97-02
hep-ph/9706382
June 1997

Hadron colliders as the "neutralino factory": Search for a slow decay of the lightest neutralino at the CERN LHC

K. Maki[1] and S. Orito[2]

Department of Physics, School of Science, University of Tokyo, Tokyo 113, Japan

Abstract

Prospects are examined for the detection of a slow decay of the lightest neutralino (or any other longlived particles) at the CERN LHC and at Very Large Hadron Collider (VLHC). We first point out that such hadron colliders will become the "neutralino factory" producing 10^6–10^9 neutralinos/yr, if gluinos and/or squarks actually exist below $O(1)$ TeV. The lightest neutralino ($\tilde{\chi}_1^0$), usually assumed to be stable, will be unstable if lighter superparticles such as the gravitino ($\tilde{G}$) or axino ($\tilde{a}$) exist, or R-parity is not conserved. The decay signal would, however, be missed in usual collider experiments, particularly when the decay mostly occurs outside the detector. In order to search for such a slow decay of $\tilde{\chi}_1^0$, we propose a dedicated experiment where the collision products are dumped by a thick shield, which is followed by a long decay tunnel. The decay product of $\tilde{\chi}_1^0$ can be detected by a detector located at the end of the tunnel. The slow arrival time and the large off angle (to the direction of the interaction point) of the decay product will provide a clear signature of slowly decaying $\tilde{\chi}_1^0$'s. One can explore the decay length ($c\tau$) in a wide range, *i.e.*, 0.2 m to 1×10^5 km for $m_{\tilde{\chi}_1^0} = 25$ GeV and 1 m to 2 km for $m_{\tilde{\chi}_1^0} = 200$ GeV at the LHC. This corresponds to the range of the SUSY breaking scale $\sqrt{F} = 2 \times 10^5$ to 2×10^7 GeV in case of the $\tilde{\chi}_1^0 \to \gamma\tilde{G}$ decay predicted in gauge-mediated SUSY breaking models. At VLHC, one can extend the explorable range of $m_{\tilde{\chi}_1^0}$ up to ~ 1000 GeV, and that of $\sqrt{F}$ up to $\sim 1 \times 10^8$ GeV. In case of the $\tilde{\chi}_1^0 \to \gamma\tilde{a}$ decay, the Peccei-Quinn symmetry breaking scale F_a can be explored up to $\sim 5 \times 10^{11}$ GeV. The mass of the decaying particle can be determined by using the correlation between the energy and the arrival time of the decay product. With the setup we propose, one can also search for (i) other decay modes of $\tilde{\chi}_1^0$ such as R-parity violating one, (ii) slow decays of any other longlived neutral or charged particles, and (iii) heavy stable charged particles.

[1]E-mail: maki@icepp.s.u-tokyo.ac.jp. Present address: Hitachi Research Laboratory, Hitachi, Ltd., 7-1-1 Omika-cho, Hitachi-shi, Ibaraki 319-12, Japan.
[2]E-mail: oriton@icepp.s.u-tokyo.ac.jp.

1 Introduction

The search for supersymmetric particles is now an integral part of all current, as well as future, experimental programs at high-energy colliders. Aside from many attractive features of supersymmetry (SUSY), the driving force for these searches comes from the recognition that weak-scale SUSY, which is introduced to solve the gauge hierarchy problem, requires that the SUSY partners of the standard model (SM) particles must be accessible to experiments that probe the TeV energy scale. If this is the case, a large number of gluinos and squarks will be produced at future hadron colliders such as the CERN LHC (operated at $\sqrt{s} = 14$ TeV with luminosity $\mathcal{L} = 10^{34}$ cm^{-2}s^{-1}) and Very Large Hadron Collider (VLHC; operated at $\sqrt{s} = 100$–200 TeV with $\mathcal{L} = 10^{34}$–10^{35} cm^{-2}s^{-1}). Once produced, gluinos and squarks will subsequently decay to the lightest neutralino ($\tilde{\chi}_1^0$). This means that such hadron colliders will become the "neutralino factory", which is capable of producing up to 10^9 $\tilde{\chi}_1^0$'s per year.

The $\tilde{\chi}_1^0$ is usually assumed to be the lightest supersymmetric particle (LSP) and thus stable if R-parity is conserved. It will then escape the detector, resulting in the famous missing energy signature for SUSY [1]. However, the $\tilde{\chi}_1^0$ might not be altogether stable: If there exists another superparticle lighter than $\tilde{\chi}_1^0$, such as the gravitino ($\tilde{G}$) or axino ($\tilde{a}$), the $\tilde{\chi}_1^0$ will decay into, *e.g.*, $\gamma\tilde{G}$ [2] or $\gamma\tilde{a}$ [3]. Such a light gravitino naturally exists in gauge-mediated SUSY breaking (GMSB) models [4–11] as well as in a class of no-scale supergravity (SUGRA) models [12]. A light axino can also exist in SUGRA models with the Peccei-Quinn (PQ) symmetry [13]. As another possibility, the violation of R-parity leads to the unstable $\tilde{\chi}_1^0$ even if it is the LSP. The $\tilde{\chi}_1^0$ will then decay into such modes as $q\bar{q}'l^{\pm}$, $q\bar{q}\nu$ and $\gamma\nu$ [14].

If the $\tilde{\chi}_1^0$ decay takes place inside the detector, the resultant event topology would be very different from that in case of the stable $\tilde{\chi}_1^0$. The experimental signatures have recently been studied for the $\tilde{\chi}_1^0$ decay into $\gamma\tilde{G}$ [15–24] and $\gamma\tilde{a}$ [25], motivated by the single $ee\gamma\gamma + \not{E}_T$ event observed in the CDF experiment at the Tevatron [26]. For the CDF event interpreted as the signal of the $\tilde{\chi}_1^0$ decay, the inferred decay length $c\tau$ is much below 1 m. However, subsequent reports on diphoton $\not{E}_T$ distribution observed in the CDF [27] and DØ [28] experiments, as well as the analysis of the LEP data at $\sqrt{s} = 161$ GeV [29], do not give any further evidence for the $\tilde{\chi}_1^0$ decay into photon(s) with such short $c\tau$. Therefore, the possibility is still open for the $\tilde{\chi}_1^0$ decay into $\gamma\tilde{G}$ or $\gamma\tilde{a}$ occurring mostly outside the detector. Actually, such a slow decay of $\tilde{\chi}_1^0$ appears to be favored at least for relatively light $\tilde{\chi}_1^0$: Original GMSB models [4] prefer relatively high SUSY breaking scale, $\sqrt{F} \gtrsim 10^7$ GeV [7], implying $c\tau(\tilde{\chi}_1^0 \to \gamma\tilde{G}) \gtrsim 100$ km for $m_{\tilde{\chi}_1^0} \lesssim 60$ GeV. In case of the $\tilde{\chi}_1^0 \to \gamma\tilde{a}$ decay, the allowed range of the PQ symmetry breaking scale, 10^9 GeV $\lesssim F_a \lesssim 10^{12}$ GeV [30, 31], leads to $c\tau \gtrsim 10$ km for $m_{\tilde{\chi}_1^0} \lesssim 60$ GeV.

If the $\tilde{\chi}_1^0$ decay is slow and mostly occurs outside the detector, the signature observed in usual collider experiments will be indistinguishable from that of the stable $\tilde{\chi}_1^0$. Hence the signal of the $\tilde{\chi}_1^0$ decay would be missed entirely. Even if a significant part of $\tilde{\chi}_1^0$'s produced at hadron colliders decay into photon(s) inside the detector, it might be hard to

detect the signature with usual detectors, because a huge number of particles produced will make it difficult to identify a single photon not coming from the interaction point. In addition, the detectors for the approved experiments at the LHC are not designed to measure the direction of each photon precisely.

Therefore, in order to search for a slow decay of $\tilde{\chi}_1^0$, we propose a dedicated experiment with the interaction point surrounded by a thick shield, by which most of the collision products are dumped. The $\tilde{\chi}_1^0$ would go through the shield and decay in a long decay tunnel. The decay product of $\tilde{\chi}_1^0$ can then be detected by a detector located at the end of the tunnel. We show that the slow arrival time and the large off angle (to the direction of the interaction point) of the decay product will provide an unambiguous signal of slowly decaying $\tilde{\chi}_1^0$'s. We also show that, in case of the $\tilde{\chi}_1^0$ decay into a photon and a light invisible particle such as $\tilde{G}$ and $\tilde{a}$, the mass of $\tilde{\chi}_1^0$ can be determined by using the correlation between the energy and the arrival time of the decay photon. Furthermore, by reconstructing the decay kinematics with the estimated decay position, one can determine whether the final state is two-body or not.

The remainder of this paper is organized as follows. We first show in Section 2 how the LHC can be the neutralino factory. In Section 3, we briefly review the theoretical models of the $\tilde{\chi}_1^0$ decay into a gravitino or an axino. Our strategy of the search for a slow decay of $\tilde{\chi}_1^0$ is then described in Section 4. In Section 5, we illustrate the method of determining the mass of $\tilde{\chi}_1^0$ after the discovery of its decay. Section 6 is devoted to the discussion of the $\tilde{\chi}_1^0$ decay search at VLHC. We also discuss in Section 7 other searches which are possible with our setup, *i.e.*, (i) other decay modes of $\tilde{\chi}_1^0$, (ii) slow decays of any other longlived neutral or charged particles, and (iii) heavy stable charged particles. Finally, we present our conclusions in Section 8. A realistic design for the detector is investigated with Monte Carlo simulations in Appendix A. In Appendix B, we estimate the rates of high-energy prompt neutrinos and muons, which can go through the iron shield and thus become the potential background.

2 The LHC as the neutralino factory

To simulate the $\tilde{\chi}_1^0$ production and decay at the LHC, we first generate various SUSY processes in pp collisions at $\sqrt{s} = 14$ TeV using ISAJET 7.13 [32] with the CTEQ2L parton distribution functions [33]. In most cases, the dominant products are the gluino ($\tilde{g}$) and squark ($\tilde{q}$), which will then decay into $\tilde{\chi}_1^0$'s through $\tilde{q} \to \tilde{g}q$ and $\tilde{g} \to q\bar{q}\tilde{\chi}_1^0$ if $m_{\tilde{q}} > m_{\tilde{g}}$, and $\tilde{g} \to \tilde{q}\bar{q}$ and $\tilde{q} \to q\tilde{\chi}_1^0$ if $m_{\tilde{q}} < m_{\tilde{g}}$. If the gluino and squark are heavy ($\gtrsim 1$ TeV), the production of gauginos (charginos and neutralinos) could become dominant. As an example, we take $m_{\tilde{q}} = 1.45\, m_{\tilde{g}}$, $\mu = -m_{\tilde{g}}$ and $\tan\beta = 2$, and assume the gaugino mass unification, which is known to roughly hold not only in SUGRA models but also in most of GMSB models.

Figure 1 shows the total cross sections for the production of gluinos, squarks and gauginos, as well as the anticipated numbers of events per 100 fb^{-1}, at the LHC as a

function of $m_{\tilde{g}}$. We note that each SUSY event contains two $\tilde{\chi}_1^0$'s in the final state. Also shown in this figure are the corresponding values of $m_{\tilde{\chi}_1^0} \approx m_{\tilde{g}}/7$, which results from the gaugino mass unification. It is worth noting that the cross sections increase by a factor up to ~ 2 when the next-to-leading order QCD corrections are properly included [34]. For the discussion below, we select three representative gluino and neutralino masses: $m_{\tilde{g}} = 300$ GeV and $m_{\tilde{\chi}_1^0} = 43$ GeV (Case 1); $m_{\tilde{g}} = 550$ GeV and $m_{\tilde{\chi}_1^0} = 78$ GeV (Case 2); and $m_{\tilde{g}} = 800$ GeV and $m_{\tilde{\chi}_1^0} = 115$ GeV (Case 3).

Figure 2 shows the angular distributions of $\tilde{\chi}_1^0$'s produced at the LHC for (a) Case 1, (b) Case 2, and (c) Case 3. The integrated luminosity is taken to be 100 fb^{-1}, which corresponds to the runtime of 10^7 s with $\mathcal{L} = 10^{34}$ cm^{-2}s^{-1}. The total numbers of produced $\tilde{\chi}_1^0$'s are 2×10^8, 8×10^6 and 9×10^5 for Case 1, 2 and 3, respectively. It can be seen that most of $\tilde{\chi}_1^0$'s are produced in the forward direction. More events can thus be detected if one installs a detector at a smaller angle θ with respect to the colliding proton beam. We here choose $\theta = 25^\circ$ (or $\cos\theta = 0.906$) for the central axis of the detector by compromising the rate of the signal and that of the potential background (high-energy prompt neutrinos and muons) as discussed in Appendix B.

Figure 3 shows the energy spectra of produced $\tilde{\chi}_1^0$'s pointing to the detector which covers $\theta = 25^\circ \pm 10^\circ$ and an elevation angle of $\pm 10^\circ$. We find that, in all three cases, the majority of $\tilde{\chi}_1^0$'s are produced with relatively low energies, *i.e.*, the energy spectra have a peak at $E_{\tilde{\chi}_1^0}/m_{\tilde{\chi}_1^0} \sim 1.5$ to 2. This means that most of the produced $\tilde{\chi}_1^0$'s are not extremely relativistic, having $\beta \equiv v/c \lesssim 0.96$. This makes the time measurement of the decay products a powerful tool for the identification of slowly decaying $\tilde{\chi}_1^0$'s.

3 Models of the lightest neutralino decay

3.1 The decay into a gravitino

Supersymmetry (SUSY) is widely acknowledged to be the best motivated extension of the SM. This is not only because it provides a natural solution to the gauge hierarchy problem, but also there exist many pieces of indirect evidence, such as the correct prediction of $\sin^2\theta_W$, the convergence of the SM gauge couplings at very high energies, and the heaviness of the top quark as required by the radiative breaking of the electroweak gauge symmetry. Moreover, SUSY can provide a plausible candidate for cosmological dark matter. These hints, as a whole, appear to constitute circumstantial evidence for SUSY.

SUSY, however, must be broken because no SUSY partners of ordinary particles have been discovered. The breaking of SUSY is usually conceived to occur in a hidden sector at some very high energies, which will probably remain unaccessible to direct collider experiments at least in the near future. Thus the investigation into the origin of the SUSY breaking is of great importance since it could be the unique window to look into the world of such high energies, perhaps up to the Planck scale. Two scenarios have been proposed on how the SUSY breaking is communicated from the hidden sector to

the observable sector: In one scenario, as in supergravity (SUGRA) models [35], SUSY breaking is mediated by gravity. In this case, the SUSY breaking scale $\sqrt{F}$ is necessarily of order 10^{11} GeV to give the superparticle masses around the weak scale. The other is the gauge-mediated SUSY breaking (GMSB) scenario [4–11], where SUSY is broken at a scale as low as 10^5–10^7 GeV, and the gauge interactions act as the messengers of SUSY breaking. Because of this relatively low value of $\sqrt{F}$, the mass degeneracy among squarks or sleptons, which results from the fact that gauge interactions are flavor blind, is hardly broken by the evolution to the weak scale, in contrast to SUGRA models. This ensures sufficient suppression of flavor changing neutral current (FCNC) processes. In addition, GMSB models may also provide a solution to the SUSY CP problem [5].

These two scenarios also lead to distinctive consequences concerning cosmological dark matter. In SUGRA models, the lightest neutralino ($\tilde{\chi}_1^0$) is usually the LSP, and can be the dominant component of dark matter. On the other hand, GMSB models naturally predict that the gravitino ($\tilde{G}$) comes out to be the LSP. The gravitino with mass ~ 0.5 keV is claimed to be a good candidate for warm dark matter [36, 37]. We note that it is practically impossible to directly detect the gravitino dark matter in laboratories, in contrast to the neutralino dark matter, whose direct detection is being pursued in many experiments.

In this way, for finding the future direction of particle physics and cosmology, it is of crucial importance to determine which scenario is realized in nature. As will be shown later, our experiment to search for a slow decay of $\tilde{\chi}_1^0$ can probe a wide range of $c\tau$, which corresponds to $\sqrt{F}$ of order 10^5 to 10^8 GeV in case of the $\tilde{\chi}_1^0 \to \gamma\tilde{G}$ decay. This covers much of the $\sqrt{F}$ range presently considered in GMSB models.

The gravitino mass $m_{\tilde{G}}$ is related to $\sqrt{F}$ (on the condition of the vanishing cosmological constant) by

$$m_{\tilde{G}} = \frac{F}{\sqrt{3}M_{\rm P}} = 2.13 \left(\frac{\sqrt{F}}{3 \times 10^6 \text{ GeV}}\right)^2 \quad \text{keV}, \tag{1}$$

where $M_{\rm P} = (8\pi G)^{-1/2} = 2.44 \times 10^{18}$ GeV is the reduced Planck mass. This leads to $m_{\tilde{G}} \simeq 0.24$ and 24 keV for $\sqrt{F} = 10^6$ and 10^7 GeV, respectively. Note that the gravitino heavier than $O(1)$ keV overcloses the Universe in the standard cosmology. Such a heavy gravitino, however, is still allowed to be the dark matter if the reheating temperature after the inflation is low enough [7, 38].

The longitudinal component of the gravitino, *i.e.*, the Goldstino, couples to matter with weak (not gravitational) interaction strength proportional to F^{-1}. Through this coupling, the $\tilde{\chi}_1^0$ will decay to a photon and a gravitino with a partial width of [2]

$$\Gamma(\tilde{\chi}_1^0 \to \gamma\tilde{G}) = \frac{\kappa_{1\gamma} m_{\tilde{\chi}_1^0}^5}{16\pi F^2}, \tag{2}$$

where $\kappa_{1\gamma}$ is the square of the photino admixture of the $\tilde{\chi}_1^0$. If the $\tilde{\chi}_1^0$ is a pure bino, $\kappa_{1\gamma} = \cos^2\theta_W \simeq 0.77$. This partial width is most likely to be the dominant one if the $\tilde{\chi}_1^0$ is the next-to-lightest supersymmetric particle (NLSP) with not too small $\kappa_{1\gamma}$, resulting

in the decay length

$$c\tau \equiv \frac{\hbar c}{\Gamma} = 80\ \kappa_{1\gamma}^{-1} \left(\frac{m_{\tilde{\chi}_1^0}}{100\ \mathrm{GeV}}\right)^{-5} \left(\frac{\sqrt{F}}{3\times 10^6\ \mathrm{GeV}}\right)^{4} \quad \mathrm{m}. \tag{3}$$

For $\sqrt{F} \gtrsim 3\times 10^6$ GeV and $m_{\tilde{\chi}_1^0} \lesssim 100$ GeV, this decay length is much longer than a typical detector size, leading that most of the decays will occur outside the detector. It has recently been pointed out [7] that such large $\sqrt{F}$ ($\gtrsim 10^7$ GeV) is expected in original GMSB models [4]. In addition, other GMSB models [8–10] tend to predict that SUSY breaking occurs at relatively high ($\gtrsim 10^6$ GeV) energies, although $\sqrt{F} = 10^5$–10^6 GeV can naturally fit in with a very recent model [11]. Equation (3) also indicates that the measurement of both $m_{\tilde{\chi}_1^0}$ and $c\tau$ will give direct information on $\sqrt{F}$.

3.2 The decay into an axino

The Peccei-Quinn (PQ) symmetry was introduced to solve the strong CP problem [39]. This symmetry should be explicitly broken, leading to a light pseudoscalar, the axion (a), whose mass is related to the PQ symmetry breaking scale F_a by

$$m_a = 6.2\times 10^{-3} \left(\frac{F_a/N}{10^9\ \mathrm{GeV}}\right)^{-1} \quad \mathrm{eV}, \tag{4}$$

where N is the QCD anomaly factor of the PQ symmetry. The axion is one of good candidates for dark matter owing to its feeble interaction with matter. The allowed range of F_a is confined to 10^9–10^{12} GeV [30, 31] from laboratory experiments as well as from astrophysical and cosmological considerations.

If both the PQ symmetry and SUSY hold in nature, there should exist the fermionic superpartner of the axion, the axino ($\tilde{a}$). The axino can remain light even after the SUSY breaking in SUGRA models [13]. In particular, the axino with mass $\sim O(1)$ keV could serve as warm dark matter [40] as is the case for the gravitino.

If such a light axino exists, the $\tilde{\chi}_1^0$ can decay into $\gamma\tilde{a}$. In case of the $\tilde{\chi}_1^0$ being a pure bino, the decay width can be written as [25]

$$\Gamma(\tilde{\chi}_1^0 \to \gamma\tilde{a}) = \frac{25\alpha_{\mathrm{em}}^2}{1152\pi^3 \cos^2\theta_W} \frac{m_{\tilde{\chi}_1^0}^3}{(F_a/N)^2}, \tag{5}$$

which corresponds to the decay length

$$c\tau = 3.6 \left(\frac{m_{\tilde{\chi}_1^0}}{100\ \mathrm{GeV}}\right)^{-3} \left(\frac{F_a/N}{10^9\ \mathrm{GeV}}\right)^{2} \quad \mathrm{km}. \tag{6}$$

The lower limit on the PQ symmetry breaking scale, $F_a \gtrsim 10^9$ GeV, implies $c\tau \gtrsim 10$ km for $m_{\tilde{\chi}_1^0} \lesssim 60$ GeV.

4 Strategy of the neutralino decay search

4.1 Dedicated experiment

We propose a completely new type of collider experiment, which is schematically shown in Fig. 4. Gluinos and squarks (and possibly gauginos) are produced in pp collisions at the interaction point and promptly decay into $\tilde{\chi}_1^0$'s. The $\tilde{\chi}_1^0$'s then enter the decay tunnel after going through the shield, by which most of the collision products are dumped. As a simple example, we here consider an iron shield of 10 m thickness, and take the tunnel length to be $L = 41.6$ m, although a much longer tunnel is certainly possible. The acceptance of the tunnel is taken to be $\theta = 25^\circ \pm 10^\circ$ and an elevation angle of $\pm 10^\circ$. We choose this angle θ by compromising the rate of the signal and that of the potential background (see Appendix B). Two layers of the anti-coincidence hodoscopes possibly with track detectors are installed just on the back end of the shield for the rejection of punchthrough muons. It can also be used for the trigger of heavy longlived charged particles. In addition, the scintillation counters and/or track detectors can be installed on the wall around the decay tunnel to reject potential background events produced by cosmic rays. If the $\tilde{\chi}_1^0$ decays to a photon and a light invisible particle in the tunnel, the decay photon will reach the end of the tunnel and enter a shower detector which has a spherical front face, and initiate the electromagnetic shower. The incident position, angle, and energy of the photon, as well as the arrival time relative to the RF clock of the accelerator, are measured by the detector.

Instead of the bulk iron shield, we can use (at extra costs) an "active" 4π-shield, consisting of segmented calorimeters, magnetized iron plates and the muon trackers. This setup will enable us to measure the total (and missing) transverse energy of the event and to tag the existence of high-energy muons.

4.2 Event simulation and the discovery signal

The decay probability of $\tilde{\chi}_1^0$ within a distance of x is given by

$$P(x) = 1 - e^{-x/\beta\gamma c\tau}, \tag{7}$$

where $\gamma \equiv E_{\tilde{\chi}_1^0}/m_{\tilde{\chi}_1^0}$ is the Lorentz factor, and $c\tau$ is the decay length. As a typical case, the probability that the $\tilde{\chi}_1^0$ with $\gamma = 2$ decays in the tunnel (10 m $\leq x \leq$ 51.6 m) is calculated to be 20% for $c\tau = 100$ m, and 2.4% for $c\tau = 1000$ m.

In the following Monte Carlo simulations, we assume that the decay photon is emitted isotropically with energy equal to $m_{\tilde{\chi}_1^0}/2$ in the rest frame of the $\tilde{\chi}_1^0$, as is the case for the $\tilde{\chi}_1^0 \to \gamma\tilde{G}$ decay with $m_{\tilde{G}} \ll m_{\tilde{\chi}_1^0}$. The photon 4-momentum $(E_\gamma, \boldsymbol{p}_\gamma)$ in the laboratory frame is then calculated by the Lorentz boost. We show in Fig. 5 a typical generated event of the $\tilde{\chi}_1^0$ decay into a photon and a light invisible particle.

Figure 6 shows the distributions of the Lorentz factor γ for $\tilde{\chi}_1^0$'s entering the decay tunnel for Case 1, 2 and 3 in (a), (b) and (c), respectively. The numbers of $\tilde{\chi}_1^0$'s entering the tunnel are 9×10^6, 4×10^5 and 5×10^4 for Case 1, 2 and 3, respectively, for total

integrated luminosity of 100 fb^{-1}, which we assume for all the simulation plots shown in this paper. The distributions of γ for $\tilde{\chi}_1^0$'s decaying in the tunnel are also shown in Fig. 6. We here take as an example the decay lengths calculated by Eq. (3) for $\sqrt{F} = 3 \times 10^6$ GeV, *i.e.*, $c\tau = 7.0$ km, 350 m, and 52 m for $m_{\tilde{\chi}_1^0} = 43$ GeV (Case 1), 78 GeV (Case 2) and 115 GeV (Case 3), respectively. The resultant numbers of $\tilde{\chi}_1^0$'s decaying in the tunnel are 1.4×10^4, 1.3×10^4 and 8×10^3 for Case 1, 2 and 3, respectively. Also shown in this figure by hatched histograms are the distributions for $\tilde{\chi}_1^0$'s whose decay photons enter the shower detector. The corresponding energy spectra of the decay photons are shown in Fig. 7 for (a) Case 1, (b) Case 2, and (c) Case 3. The spectra have a peak at $E_\gamma \sim m_{\tilde{\chi}_1^0}$ and extend up to ~ 1000 GeV.

The clear separation of the $\tilde{\chi}_1^0$ decay signal from the potential background, *i.e.*, high-energy prompt neutrinos and muons as well as the cosmic-ray events, can be attained by measuring the arrival time and the off angle ψ to the direction of the interaction point (see Fig. 4). Figure 8 shows the scatter plots of ψ vs. the arrival time for (a) Case 1, (b) Case 2, (c) Case 3, and (d) background neutrinos and muons (ν/μ). The background ν/μ events all have $\psi \simeq 0^\circ$, and arrive in narrow bunch structure (here we assume $\sigma_t = 0.2$ ns). On the other hand, most of the decay photons have large ψ (up to $\sim 30^\circ$) and arrive with significant delay (typically 1–20 ns), because most of the produced $\tilde{\chi}_1^0$'s are not extremely relativistic. We show in Fig. 9 the arrival time distributions. The evidence for a slow decay of the heavy parent particles is clear in the peak position, which is displaced by about 2 ns from the exact bunch position, as well as in the long tail after the peak.

The decay length $c\tau$ can in principle be estimated from the distribution of the events in the scatter plot of ψ vs. the arrival time. Moreover, one could measure $c\tau$ from the variation of the signal count rate correlated with the change of L, which can be performed by moving the detector on rails. Together with the measured value of $m_{\tilde{\chi}_1^0}$ (see Section 5), one can determine the strength of the interaction which governs the $\tilde{\chi}_1^0$ decay. In particular, if one interprets the observed events as the $\tilde{\chi}_1^0 \to \gamma\tilde{G}$ ($\tilde{\chi}_1^0 \to \gamma\tilde{a}$) decay, the SUSY breaking scale $\sqrt{F}$ (the PQ symmetry breaking scale F_a) can be determined.

4.3 Explorable range of the decay length at the LHC

The large off angle ψ and the slow arrival time are the generic features of slowly decaying heavy particles, and will thus always provide a clear signature of slowly decaying $\tilde{\chi}_1^0$'s. Based on this prospect, we now estimate the explorable range of the decay length $c\tau$.

Figures 8 and 9 represent typical examples of the off angle ψ and the arrival time distributions for $c\tau$ much longer than (Cases 1 and 2) or comparable to (Case 3) the tunnel length. For longer $c\tau$, the characteristic shape of the distribution will not change, while the number of detected events will decrease in proportion to $(c\tau)^{-1}$. In order to estimate the longest explorable decay length, we assume that 10 events with such a characteristic distribution are enough to discover the signal.

For $c\tau$ much shorter than the tunnel length, most of the detected events will be due to the $\tilde{\chi}_1^0$ decaying immediately after going through the shield. Such events will show the

smaller off angle and shorter arrival time as compared to the cases shown in Figs. 8 and 9. The off angle will nevertheless have finite non-zero values (typically of 1 to 10°), and the arrival time will definitely be deviated (by 1 to 10 ns) from that of background ν/μ events, because the $\tilde{\chi}_1^0$ flies at least the shield thickness before decaying. In estimating the shortest explorable decay length, we assume 100 such events are enough to discover the signal.

Figure 10 shows the resultant explorable range of $c\tau$ for various $m_{\tilde{\chi}_1^0}$ at the LHC with 300 fb^{-1}. It can be seen that the explorable range of $c\tau$ is wide, *i.e.*, 0.2 m to 1×10^5 km for $m_{\tilde{\chi}_1^0} = 25$ GeV, and 1 m to 2 km for $m_{\tilde{\chi}_1^0} = 200$ GeV. We also show in this figure the predicted curves of $c\tau$ for the $\tilde{\chi}_1^0$ decay into $\gamma\tilde{G}$ and $\gamma\tilde{a}$ for typical values of $\sqrt{F}$ and F_a, respectively. We find that one can explore $\sqrt{F}$ in a wide range of 2×10^5 to 2×10^7 GeV through the $\tilde{\chi}_1^0 \to \gamma\tilde{G}$ decay. This range includes an interesting case of $\sqrt{F} \sim 10^6$ GeV, where the gravitino has mass ~ 0.5 keV and can be the dominant component of dark matter in the standard cosmology. In case of the $\tilde{\chi}_1^0 \to \gamma\tilde{a}$ decay, F_a can be explored up to $\sim 10^{10}$ GeV for $m_{\tilde{\chi}_1^0} \lesssim 60$ GeV.

5 Determination of the neutralino mass and decay kinematics

After discovering the signal of the $\tilde{\chi}_1^0$ decay, one can determine the mass of $\tilde{\chi}_1^0$ by using the correlation between the energy and the arrival time of the decay photon, if enough number of decay events can be accumulated.

For this purpose, we first extract the approximate time-of-flight (TOF) of $\tilde{\chi}_1^0$, $t_{\rm TOF}$, from the time difference between the signal of the shower detector and the RF clock of the accelerator, as illustrated in Fig. 11. In this process, we assume that each $\tilde{\chi}_1^0$ comes from the closest possible bunch of the proton beam on the condition of $\beta \leq 1$. The probability of attributing an event to a wrong starting bunch is small, *i.e.*, 20–25% for the three cases described above. Using the extracted value of $t_{\rm TOF}$, we define the parameter β_* as

$$\beta_* \equiv \frac{|\overrightarrow{\rm OE}|}{c\, t_{\rm TOF}}, \tag{8}$$

where $|\overrightarrow{\rm OE}|$ is the distance from the interaction point to the front face of the shower detector. The distributions of β_*^{-1} are shown in Fig. 12 for (a) Case 1, (b) Case 2, (c) Case 3, and (d) background ν/μ. There is an upper cutoff at $\beta_*^{-1} \sim 1.15$, which results from the modulation of $t_{\rm TOF}$ by the bunch spacing of 25 ns. The background ν/μ events make a sharp peak at $\beta_*^{-1} \sim 1$ with no tail in contrast to the $\tilde{\chi}_1^0$ decay signal.

Figure 13 shows the scatter plots of E_γ vs. $\gamma_* \equiv (1-\beta_*^2)^{-1/2}$ for (a) Case 1, (b) Case 2, and (c) Case 3. The photon energy resolution is assumed to be $\sigma_E/E = 33\%/\sqrt{E\ ({\rm GeV})}$. The lower cutoff of γ_* at ~ 2 corresponds to the above-mentioned cutoff of β_*^{-1} at ~ 1.15. One can also find an edge with constant ratio of E_γ to γ_*. This edge is composed of the events in which the decay occurs near the front face of the shower detector with the decay

photon emitted toward the flight direction of the $\tilde{\chi}_1^0$. For such events, $|\overrightarrow{\mathrm{OE}}|$ and t_{TOF} are nearly the same as the actual flight length and TOF of the $\tilde{\chi}_1^0$, respectively, and the decay photon has the full energy of the $\tilde{\chi}_1^0$, *i.e.*, $E_\gamma \approx E_{\tilde{\chi}_1^0}$, resulting in the edge corresponding with $E_\gamma/\gamma_* = m_{\tilde{\chi}_1^0}$. From the position of this edge, the mass of $\tilde{\chi}_1^0$ can be determined with an accuracy of $\lesssim 20\%$. For this purpose, the shower detector should be designed to measure the photon energy in a wide range of 10 to 1000 GeV. Figure 14 shows the corresponding distributions of E_γ/γ_* for Cases 1 to 3. An upper endpoint at $E_\gamma/\gamma_* = m_{\tilde{\chi}_1^0}$ can be seen in each case.

We now try to determine the nature of the $\tilde{\chi}_1^0$ decay, *i.e.*, whether it is two-body or not. Although the symmetric peak at $E_\gamma/\gamma_* = m_{\tilde{\chi}_1^0}/2$ in Fig. 14 may be the first hint of the two-body decay, we can prove the two-body nature by directly reconstructing the decay kinematics. For this purpose, we first select events with $\psi \geq 10^\circ$ based on the ψ distribution shown in Fig. 15 for (a) Case 1, (b) Case 2, (c) Case 3, and (d) background ν/μ. After this ψ cut, only events in which the $\tilde{\chi}_1^0$ decays relatively near the shower detector can survive. The efficiency of this cut is $\sim 40\%$ for each of the three cases.

Figure 16 shows the scatter plots of E_γ vs. γ_* for Cases 1 to 3 after the cut of $\psi \geq 10^\circ$. It can be seen that only photons with relatively low energies survive. Thus the two methods of determining the $\tilde{\chi}_1^0$ mass, *i.e.*, the use of the edge in the scatter plot of E_γ vs. γ_*, and the direct reconstruction of the decay kinematics, are complementary in that different events are mainly used in these two methods.

We then simply assume that the decay position D is the middle point between C and E, both of which are defined in Fig. 4. Using this assumption, the velocity of the $\tilde{\chi}_1^0$ can be approximately expressed by

$$\beta_{\mathrm{obs}} = \frac{|\overrightarrow{\mathrm{OD}}|}{c\,t_{\mathrm{TOF}} - |\overrightarrow{\mathrm{DE}}|}, \tag{9}$$

where $|\overrightarrow{\mathrm{OD}}|$ and $|\overrightarrow{\mathrm{DE}}|$ represent the flight path of the $\tilde{\chi}_1^0$ and that of the photon, respectively. One can then calculate the reconstructed mass as

$$M_{\gamma\tilde{G}} \equiv E_\gamma(1 - \beta_{\mathrm{obs}}\cos\theta_{\mathrm{lab}})(1 - \beta_{\mathrm{obs}}^2)^{-1/2}, \tag{10}$$

where θ_{lab} is the angle between the momentum of the $\tilde{\chi}_1^0$ and that of the photon (see Fig. 4). Figure 17 shows the distributions of $M_{\gamma\tilde{G}}$ for (a) Case 1, (b) Case 2, and (c) Case 3. It can be seen that the $\tilde{\chi}_1^0$ mass can be determined with an accuracy of $\sim 30\%$ for each case. If one finds a peak in the distribution of $M_{\gamma\tilde{G}}$ at the right position expected from the edge in the scatter plot of E_γ vs. γ_*, one can conclude that the observed events are really the signature of the two-body decay of $\tilde{\chi}_1^0$ into a photon and an invisible particle.

6 Prospects for the neutralino decay search at VLHC

Very Large Hadron Collider (VLHC) [41] has been discussed recently as a post-LHC machine, being operated at $\sqrt{s} = 100$–200 TeV with $\mathcal{L} = 10^{34}$–10^{35} cm^{-2}s^{-1}. We stress

here that the VLHC will become the neutralino factory much more powerful than the LHC. Figure 18 shows the total cross sections for the production of gluinos, squarks and gauginos, as well as the anticipated numbers of events per 1000 fb^{-1}, in pp collisions at $\sqrt{s} = 100$ TeV as a function of $m_{\tilde{g}}$. Also shown in this figure are the corresponding values of $m_{\tilde{\chi}_1^0} \approx m_{\tilde{g}}/7$.

Figure 19 shows the explorable range of $c\tau$ for the $\tilde{\chi}_1^0$ decay at the VLHC with 3000 fb^{-1}. As in Fig. 10, the upper end of the explorable region corresponds to the level of 10 decay events detected, and the lower one is derived from the condition that 100 decay events are detected. The explorable range of $c\tau$ is found to be 0.1 m to 1×10^7 km for $m_{\tilde{\chi}_1^0} = 25$ GeV, 0.2 m to 5×10^3 km for $m_{\tilde{\chi}_1^0} = 200$ GeV, and 1 m to 1 km for $m_{\tilde{\chi}_1^0} = 1000$ GeV. We also show in this figure the predicted curves of $c\tau$ for the $\tilde{\chi}_1^0 \to \gamma\tilde{G}$ and $\tilde{\chi}_1^0 \to \gamma\tilde{a}$ decays for typical values of $\sqrt{F}$ and F_a, respectively. It is found that one can extend the reach for $\sqrt{F}$ up to 1×10^8 GeV through the $\tilde{\chi}_1^0 \to \gamma\tilde{G}$ decay. In case of the $\tilde{\chi}_1^0 \to \gamma\tilde{a}$ decay, F_a can be explored up to $\sim 5 \times 10^{11}$ GeV for relatively light $\tilde{\chi}_1^0$. It is worth noting that our experiment is unique in that one can explore such a high value of F_a in laboratories. In addition, our experiment can be performed under very high luminosity exceeding 10^{35} cm^{-2}s^{-1}, in contrast to usual collider experiments.

7 Other possible searches

7.1 Other decay modes of the lightest neutralino

One can search for other modes of the $\tilde{\chi}_1^0$ decay by using the setup proposed in this paper. If the $\tilde{\chi}_1^0$ is sufficiently heavy, it can decay into $Z^0\tilde{G}$ or $h^0\tilde{G}$ (where h^0 is the Higgs boson) in the gravitino LSP scenario [17, 18]. In case the $\tilde{\chi}_1^0$ is higgsino-like, the $h^0\tilde{G}$ decay can even be dominant. Since the Z^0 and h^0 bosons subsequently decay into $q\bar{q}$ or l^+l^-, the visible signature of these $\tilde{\chi}_1^0$ decays will be two hadron jets or two leptons without any signal in the anti-coincidence hodoscopes. With the help of track detectors at the end of the decay tunnel, the decay point can be exactly located, which makes the kinematical analysis of the decay and the mass determination much more streightforward than in case of the $\tilde{\chi}_1^0 \to \gamma\tilde{G}$ decay described in Section 5. The $\tilde{\chi}_1^0$ can also decay into such modes as $q\bar{q}'l^\pm$, $q\bar{q}\nu$ and $\gamma\nu$ through weak violation of R-parity [14]. Furthermore, the decay of other longlived neutral particles, *e.g.* heavy neutrinos, can be detected with the same setup and method.

7.2 Slow decays of longlived charged particles

Our setup can also be used to search for slow decays of heavy longlived charged particles. Although the existence of such particles would in principle be indicated in collider experiments by charged particle tracks with ionization larger than the minimum one, the signature of their decay will be missed if it occurs mostly outside the detector. On the other hand, with our setup, one can clearly detect the decay signal of such longlived par-

ticles as in case of the $\tilde{\chi}_1^0$ decay. The "anti-coincidence" hodoscopes can be used as the trigger counter.

There are several candidates for longlived charged particles in SUSY models. For example, if the gravitino or axino is the LSP, a charged superparticle such as the slepton ($\tilde{l}^-$) can be the NLSP, and may decay into $l^-\tilde{G}$ with $c\tau$ much longer than the detector size. The chargino ($\tilde{\chi}_1^-$) can be another example of the longlived NLSP if the mass difference between the $\tilde{\chi}_1^-$ and the $\tilde{\chi}_1^0$ (assumed to be the LSP) is so small that it can decay only via $\tilde{\chi}_1^- \to e^-\bar{\nu}_e\tilde{\chi}_1^0$ [42]. Weak violation of R-parity would also allow the existence of longlived charged particles [43]. In this case, the slepton can be the LSP, decaying slowly via, *e.g.*, $\tilde{l}^- \to l^-\nu$. Furthermore, heavy longlived charged particles could also exist in the SUSY breaking sector and messenger sectors of GMSB models [10, 44]. There are also many other speculations on heavy longlived charged particles [45–48].

7.3 Heavy stable charged particles

If the $c\tau$ of heavy charged particles is extremely long, they will appear to be "stable" particles even in our experiment. One can search for such particles with our setup by precisely measuring their time-of-flight over 40 m distance between the "anti-coincidence" hodoscopes and the shower detector at the end of the tunnel. The β^{-1} distribution for heavy stable charged particles is expected to have a long tail following the peak at $\beta^{-1} \sim 1$, in contrast to muons which make a sharp peak at $\beta^{-1} = 1$. Long flight path in our setup leads to excellent resolution of β, which will provide a clear signal for the heavy stable charged particle. One could then determine its mass by measuring its momentum with magnetized iron and tracking chambers, which can be installed either in the active shield or at the very end of the shower detector.

8 Conclusions

We have investigated the detection of a slow decay of the lightest neutralino (or any other longlived particles) at the CERN LHC and at VLHC. After pointing out that such hadron colliders will become the "neutralino factory" producing 10^6–10^9 $\tilde{\chi}_1^0$'s/yr if SUSY particles actually exist below $O(1)$ TeV, we have shown that a slow decay of $\tilde{\chi}_1^0$ can be detected in a dedicated experiment in which the collision products are dumped by a thick shield. The decay product of $\tilde{\chi}_1^0$ can then be detected by a detector located at the end of a long decay tunnel. The slow arrival time and the large off angle ψ of the decay product will provide a clear signature of slowly decaying $\tilde{\chi}_1^0$'s. Considering the $\tilde{\chi}_1^0$ decay into a photon and a light invisible particle such as the gravitino ($\tilde{G}$) or axino ($\tilde{a}$), we find that one can explore the decay length ($c\tau$) of $\tilde{\chi}_1^0$ in a wide range, *i.e.*, 0.2 m to 1×10^5 km for $m_{\tilde{\chi}_1^0} = 25$ GeV and 1 m to 2 km for $m_{\tilde{\chi}_1^0} = 200$ GeV for the case of the LHC. This corresponds to the range of the SUSY breaking scale $\sqrt{F} = 2 \times 10^5$ to 2×10^7 GeV in case of the $\tilde{\chi}_1^0 \to \gamma\tilde{G}$ decay. At VLHC, one can extend the explorable range of $m_{\tilde{\chi}_1^0}$ up to ~ 1000 GeV, and that of $\sqrt{F}$ up to $\sim 1 \times 10^8$ GeV. In case of the $\tilde{\chi}_1^0 \to \gamma\tilde{a}$ decay, one can explore the PQ

symmetry breaking scale F_a up to $\sim 5 \times 10^{11}$ GeV. The mass of the decaying particle can be determined with an accuracy of $\lesssim 20\%$ using the correlation between the energy and the arrival time of the decay photon. With the setup we propose, one can also search for (i) other decay modes of $\tilde{\chi}_1^0$ such as R-parity violating one, (ii) the decay of any other longlived neutral or charged particles, and (iii) heavy stable charged particles.

The experiment we proposed in this paper is a completely new type of collider experiment, which may turn out to be of crucial importance. The civil engineering of the intersection region at future hadron colliders has to be designed so that it can accommodate long decay tunnels for such experiments.

Acknowledgements

All the calculations were performed on the RS/6000 workstations of the International Center for Elementary Particle Physics (ICEPP), University of Tokyo. K.M. acknowledges a fellowship from the Japan Society for the Promotion of Science.

Appendixes

A Realistic design for the shower detector

Figure 20 shows a schematical view of a realistic design for the shower detector which we have investigated. To separate electromagnetic showers initiated by photons from the background, we design the detector consisting of the preshower detector (PS), two parts of the electromagnetic calorimeter (EM1 and EM2), three planes of plastic scintillators (S1, S2 and S3), the lead absorber (L1), and the hadron calorimeter (HAD). In addition, we can install the tracking chambers both in front of and behind the whole detector for the definite detection of high-energy muons (and possibly heavy stable charged particles).

The preshower detector (PS) comprises two planes of multiwire proportional chambers (MWPCs) with cathode pad readout, with $2X_0$ and $1X_0$ lead converter in front, respectively (radiation length X_0 being 0.56 cm for lead). The scintillator S1 in front of PS can work as the anti-coincidence counter for charged particles. The scintillator S2, located just behind PS, is used for triggering. The electromagnetic calorimeter is divided into two parts, each of which comprises modules with 10×10 cm^2 transverse dimensions. The first part (EM1), which is located at 170 cm downstream of PS, consists of 5 layers of lead ($1X_0$) and scintillators (1 cm). The second part (EM2), which is located at 220 cm downstream of EM1, consists of 20 layers of lead ($1X_0$) and scintillators (1 cm). Total radiation lengths of EM1 and EM2 are $5.1X_0$ and $20.4X_0$, respectively. The thick scintillator S3, located between EM1 and EM2, is used not only for triggering but also for the measurement of the arrival time. The hadron calorimeter (HAD) contains 15 layers of 5 cm thick iron and 2 cm thick scintillators. Total thickness is ~ 5 nuclear interaction lengths. Hadronic showers will deposit much of its energy in HAD. Between

EM2 and HAD, the lead absorber L1 of $20X_0$ in thickness is inserted to totally absorb electromagnetic showers.

A coincidence of two planes of scintillators, *i.e.* S2 and S3, constitutes the first trigger. We also require the signals from EM1 and EM2 to exceed a threshold, which leads to the rejection of (i) muons going through the detector as minimum ionizing particles, and (ii) hadronic showers initiated by high-energy neutrinos in HAD.

For this detector configuration, we have performed Monte Carlo simulations using GEANT 3.21 [49]. A typical event for 100 GeV photon incident on the shower detector is shown in Fig. 21. We can see that the electromagnetic shower starts to evolve in PS, reaches its maximum after passing EM1, and is mostly absorbed in EM2. Figure 22 shows the distributions of energy deposited in active layers of (a) S2, (b) EM1, (c) EM2, and (d) HAD, by 100 GeV photons and charged pions which are incident at 0° on the shower detector. It can be seen that electromagnetic showers (initiated by photons) can clearly be separated from hadronic showers (initiated by pions) using the deposit energy of each component.

The energy of incident photons can be determined from the sum of deposit energy in active layers of EM1 and EM2, denoted as $E_{\rm EM1} + E_{\rm EM2}$, whose distributions are shown in Fig. 23(a) for photons incident at 0° with energy E = 20, 50, 100 and 200 GeV. The inefficiency concerning the scintillation light collection is not included. Figure 23(b) shows the relation between E and $E_{\rm EM1} + E_{\rm EM2}$ for 0° and 30° incidence. It can be seen that good linearity is realized for E = 20–200 GeV. The resultant energy resolution of the shower detector as a function of incident photon energy is shown in Fig. 23(c). The fit result for 0° data is $\sigma_E/E = 32.6\%/\sqrt{E\ ({\rm GeV})}$ for E = 20–200 GeV.

The shower direction is obtained from the reconstructed position of the shower in PS and that in EM2. The position of the shower in PS can be determined from the pad signal of MWPCs, whose spatial resolution is assumed to be 5 mm. The shower center in EM2 can be estimated from the observed division of energy within a local cluster of modules. We find that good spatial resolution ($\sigma_{x,y} \sim 2$ cm) in comparison with the size of the module (10×10 cm^2) can be obtained owing to the large gap between EM1 and EM2, which makes the shower spread widely before entering EM2. The resultant angular resolution averaged over various incident positions is shown in Fig. 24. It is found to be $\sigma_\theta \lesssim 0.3°$ for photons with E = 50–200 GeV. The angular resolution could be improved if tracking chambers are used as active layers of EM1 and EM2 instead of scintillators.

B Rates of high-energy neutrinos and muons

Although a large number of particles will be produced at the LHC, most of them (hadrons, $e^\pm$ and γ) will be dumped in our setup by the iron shield with thickness of ~ 60 nuclear interaction lengths. However, high-energy neutrinos and muons can go through the shield and might interact with the material of the detector. The main source of high-energy neutrinos and muons is expected to be "prompt", *i.e.*, come from semileptonic decays

of bottom and charm hadrons [50], while the contribution from the decay of π and K mesons is negligible at least in our setup. In order to estimate the rates of these prompt neutrinos and muons, we have performed Monte Carlo simulations using ISAJET 7.13 [32] for pp collisions at $\sqrt{s} = 14$ TeV, by taking the total cross section of the bottom plus charm production to be 2 mb. Total 2.4×10^6 events are generated, and the neutrinos and muons which point to the detector covering a polar angle of $\theta_{\rm axis} \pm 10^\circ$ and an elevation angle of $\pm 10^\circ$ are recorded. We consider four cases, *i.e.*, $\theta_{\rm axis} = 15^\circ$, 20°, 25° and 30°.

B.1 Interacting neutrinos

The energy spectra of the prompt neutrinos are shown in Fig. 25. The spectra have a long high-energy tail when $\theta_{\rm axis}$ is small. The neutrino could mimic the $\gamma\tilde{G}$ or $\gamma\tilde{a}$ signal if it interacts in the preshower detector and deposits enough energy (see Appendix A for the detailed design for the shower detector). As a simple estimate of such background, we calculate the number of neutrinos which have energy $E_\nu \geq 20$ GeV and interact with $3X_0 \approx 19$ g/cm^2 lead. The interaction cross section is taken to be $5 \times 10^{-39} (E_\nu/{\rm GeV})$ cm^2/nucleon. The estimated numbers are ~ 0.2, ~ 0.02, $\lesssim 0.01$ and $\lesssim 0.001$ per 100 fb^{-1} for $\theta_{\rm axis} = 15^\circ$, 20°, 25° and 30°, respectively. Thus the background induced by the prompt neutrinos is negligibly small.

B.2 Muon-induced background

Figure 26 shows the energy spectra of the prompt muons. Only the muons with $E_\mu \geq 20$ GeV can go through the shield because of the ionization energy loss. The resultant rates of muons entering the tunnel are then estimated to be ~ 5 kHz, ~ 600 Hz, $\lesssim 200$ Hz and $\lesssim 80$ Hz for $\theta_{\rm axis} = 15^\circ$, 20°, 25° and 30°, respectively, with luminosity of 10^{34} cm^{-2}s^{-1}. The single rate of the prompt muons will thus be comfortably small if we take $\theta_{\rm axis} \gtrsim 25^\circ$.

High-energy muons can deposit a significant portion of their energy by bremsstrahlung or direct e^+e^- pair production, both of which could lead to the electromagnetic shower. When combined with inefficiencies in the anti-coincidence counters, these muons might in principle mimic the $\gamma\tilde{G}$ or $\gamma\tilde{a}$ signal. Folding the simulated spectra by the showering probability [51] of muons, we estimate the numbers of muon-induced high-energy ($E \geq 10$ GeV) showers starting to evolve in the preshower detector to be $\sim 10^7$, $\sim 10^6$, $\lesssim 2 \times 10^5$ and $\lesssim 10^5$ per 100 fb^{-1} for $\theta_{\rm axis} = 15^\circ$, 20°, 25° and 30°, respectively. Assuming a veto inefficiency of $\sim 10^{-6}$ by the staggered layers of anti-coincidence scintillators, the muon-induced background is expected to be negligibly small for $\theta_{\rm axis} \gtrsim 25^\circ$.

Even if the rate of such muon-induced background turns out to be non-negligible, off-line analysis will eliminate such background based on the information on the arrival time as well as on the off angle ψ.

References

[1] H. Baer, C-H. Chen, F. Paige and X. Tata, Phys. Rev. D **52**, 2746 (1995); Phys. Rev. D **53**, 6241 (1996).

[2] N. Cabibbo, G.R. Farrar and L. Maiani, Phys. Lett. **105B**, 155 (1981).

[3] J.F. Nieves, Phys. Lett. B **174**, 411 (1986).

[4] M. Dine and A.E. Nelson, Phys. Rev. D **48**, 1277 (1993); M. Dine, A.E. Nelson and Y. Shirman, Phys. Rev. D **51**, 1362 (1995); M. Dine, A.E. Nelson, Y. Nir and Y. Shirman, Phys. Rev. D **53**, 2658 (1996).

[5] M. Dine, Y. Nir and Y. Shirman, Phys. Rev. D **55**, 1501 (1997).

[6] G. Dvali, G.F. Giudice and A. Pomarol, Nucl. Phys. **B478**, 31 (1996); A.E. Faraggi, Phys. Lett. B **387**, 775 (1996); S.P. Martin, Phys. Rev. D **55**, 3177 (1997); S. Dimopoulos and G.F. Giudice, Phys. Lett B **393**, 72 (1997).

[7] A. de Gouvêa, T. Moroi and H. Murayama, Report No. hep-ph/9701244 (unpublished).

[8] T. Hotta, Izawa K.-I. and T. Yanagida, Phys. Rev. D **55**, 415 (1997); L. Randall, Report No. hep-ph/9612426 (unpublished); N. Haba, N. Maru and T. Matsuoka, Report No. hep-ph/9612468 (unpublished); hep-ph/9703250 (unpublished); Y. Shadmi, Report No. hep-ph/9703312 (unpublished).

[9] E. Poppitz and S.P. Trivedi, Phys. Rev. D **55**, 5508 (1997); Phys. Lett. B **401**, 38 (1997).

[10] N. Arkani-Hamed, H. Murayama and J. March-Russell, Report No. hep-ph/9701286 (unpublished); H. Murayama, Report No. hep-ph/9705271 (unpublished).

[11] Izawa K.-I., Y. Nomura, K. Tobe and T. Yanagida, Report No. hep-ph/9705228 (unpublished).

[12] J. Ellis, K. Enqvist and D.V. Nanopoulos, Phys. Lett. **147B**, 99 (1984).

[13] T. Goto and M. Yamaguchi, Phys. Lett. B **276**, 103 (1992); E.J. Chun, J.E. Kim and H.P. Nilles, Phys. Lett. B **287**, 123 (1992); E.J. Chun and A. Lukas, Phys. Lett. B **357**, 43 (1995).

[14] L.J. Hall and M. Suzuki, Nucl. Phys. **B231**, 419 (1984); S. Dawson, Nucl. Phys. **B261**, 297 (1985); R. Barbieri and A. Masiero, Nucl. Phys. **B267**, 679 (1986); H. Dreiner and G.G. Ross, Nucl. Phys. **B365**, 597 (1991).

[15] K. Kiers, J.N. Ng and G. Wu, Phys. Lett. B **381**, 177 (1996).

[16] D.R. Stump, M. Wiest and C.-P. Yuan, Phys. Rev. D **54**, 1936 (1996).

[17] S. Dimopoulos, M. Dine, S. Raby and S. Thomas, Phys. Rev. Lett. **76**, 3494 (1996); S. Dimopoulos, S. Thomas and J.D. Wells, Phys. Rev. D **54**, 3283 (1996); S. Dimopoulos, M. Dine, S. Raby, S. Thomas and J.D. Wells, Nucl. Phys. Proc. Suppl. **52A**, 38 (1997).

[18] S. Ambrosanio, G.L. Kane, G.D. Kribs, S.P. Martin and S. Mrenna, Phys. Rev. Lett. **76**, 3498 (1996); Phys. Rev. D **54**, 5395 (1996); S. Ambrosanio, G.D. Kribs and S.P. Martin, Report No. hep-ph/9703211 (unpublished).

[19] K.S. Babu, C. Kolda and F. Wilczek, Phys. Rev. Lett. **77**, 3070 (1996).

[20] J.A. Bagger, K. Matchev, D.M. Pierce and R. Zhang, Phys. Rev. D **55**, 3188 (1997).

[21] H. Baer, M. Brhlik, C-H. Chen and X. Tata, Phys. Rev. D **55**, 4463 (1997).

[22] F.M. Borzumati, Report No. hep-ph/9702307 (unpublished).

[23] D.A. Dicus, B. Dutta and S. Nandi, Phys. Rev. Lett. **78**, 3055 (1997); Report No. hep-ph/9704225 (unpublished).

[24] J.L. Lopez and D.V. Nanopoulos, Mod. Phys. Lett. A **11**, 2473 (1996); Phys. Rev. D **55**, 4450 (1997); J.L. Lopez, D.V. Nanopoulos and A. Zichichi, Phys. Rev. Lett. **77**, 5168 (1996); Report No. hep-ph/9610235 (unpublished); Phys. Rev. D **55**, 5813 (1997).

[25] J. Hisano, K. Tobe and T. Yanagida, Phys. Rev. D **55**, 411 (1997).

[26] S. Park, in *Proceedings of the 10th Topical Workshop on Proton-Antiproton Collider Physics, Fermilab, 1995*, edited by R. Raja and J. Yoh (AIP, New York, 1995) p. 62.

[27] D. Toback, Report No. FERMILAB-Conf-96/240-E (unpublished).

[28] S. Abachi *et al.*, Phys. Rev. Lett. **78**, 2070 (1997).

[29] J. Ellis, J.L. Lopez and D.V. Nanopoulos, Phys. Lett. B **394**, 354 (1997).

[30] See, *e.g.*, E.W. Kolb and M.S. Turner, *The Early Universe* (Addison-Wesley, 1990).

[31] H.-T. Janka, W. Keil, G. Raffelt and D. Seckel, Phys. Rev. Lett. **76**, 2621 (1996); G. Sigl, Phys. Rev. Lett. **76**, 2625 (1996).

[32] H. Baer, F.E. Paige, S.D. Protopopescu and X. Tata, in *Proceedings of the Workshop on Physics at Current Accelerators and Supercolliders*, edited by J. Hewett, A. White and D. Zeppenfeld (Argonne National Laboratory, Argonne, 1993).

[33] J. Botts *et al.*, Phys. Lett. B **304**, 159 (1993); H.L. Lai *et al.*, Phys. Rev. D **51**, 4763 (1995).

[34] W. Beenakker, R. Höpker, M. Spira and P.M. Zerwas, Nucl. Phys. B **492**, 51 (1997).

[35] See, *e.g.*, H.P. Nilles, Phys. Rep. **110**, 1 (1984).

[36] H. Pagels and J.R. Primack, Phys. Rev. Lett. **48**, 223 (1982); M. Kawasaki, N. Sugiyama and T. Yanagida, Report No. hep-ph/9607273 (unpublished).

[37] S. Borgani, A. Masiero and M. Yamaguchi, Phys. Lett. B **386**, 189 (1996).

[38] T. Moroi, H. Murayama and M. Yamaguchi, Phys. Lett. B **303**, 289 (1993).

[39] R.D. Peccei and H.R. Quinn, Phys. Rev. Lett. **38**, 1440 (1977); Phys. Rev. D **16**, 1791 (1977).

[40] K. Rajagopal, M.S. Turner and F. Wilczek, Nucl. Phys. B **358**, 447 (1991).

[41] D. Denisov and S. Keller, Report No. hep-ph/9701402 (unpublished).

[42] C.-H. Chen, M. Drees and J.F. Gunion, Phys. Rev. D **55**, 330 (1997).

[43] N.V. Krasnikov, Phys. Lett. B **386**, 161 (1996).

[44] S. Dimopoulos, G.F. Giudice and A. Pomarol, Phys. Lett. B **389**, 37 (1996); G. Dvali and M. Shifman, Phys. Lett. B **399**, 60 (1997).

[45] R. Barbieri, G. Dvali and A. Strumia, Nucl. Phys. **B391**, 487 (1993).

[46] C.T. Hill and E.A. Paschos, Phys. Lett. B **241**, 96 (1990).

[47] J. Maalampi and M. Roos, Phys. Rep. **186**, 53 (1990).

[48] J.L. Hewett and T.G. Rizzo, Phys. Rep. **183**, 193 (1989).

[49] Application Software Group, CERN Program Library Long Writeup W5013, 1993 (unpublished).

[50] ATLAS Collaboration, ATLAS Technical Proposal, Report No. CERN/LHCC/94-43 (1994).

[51] Y.S. Tsai, Rev. Mod. Phys. **46**, 815 (1974); A. van Ginneken, Nucl. Instr. Meth. A **251**, 21 (1986).

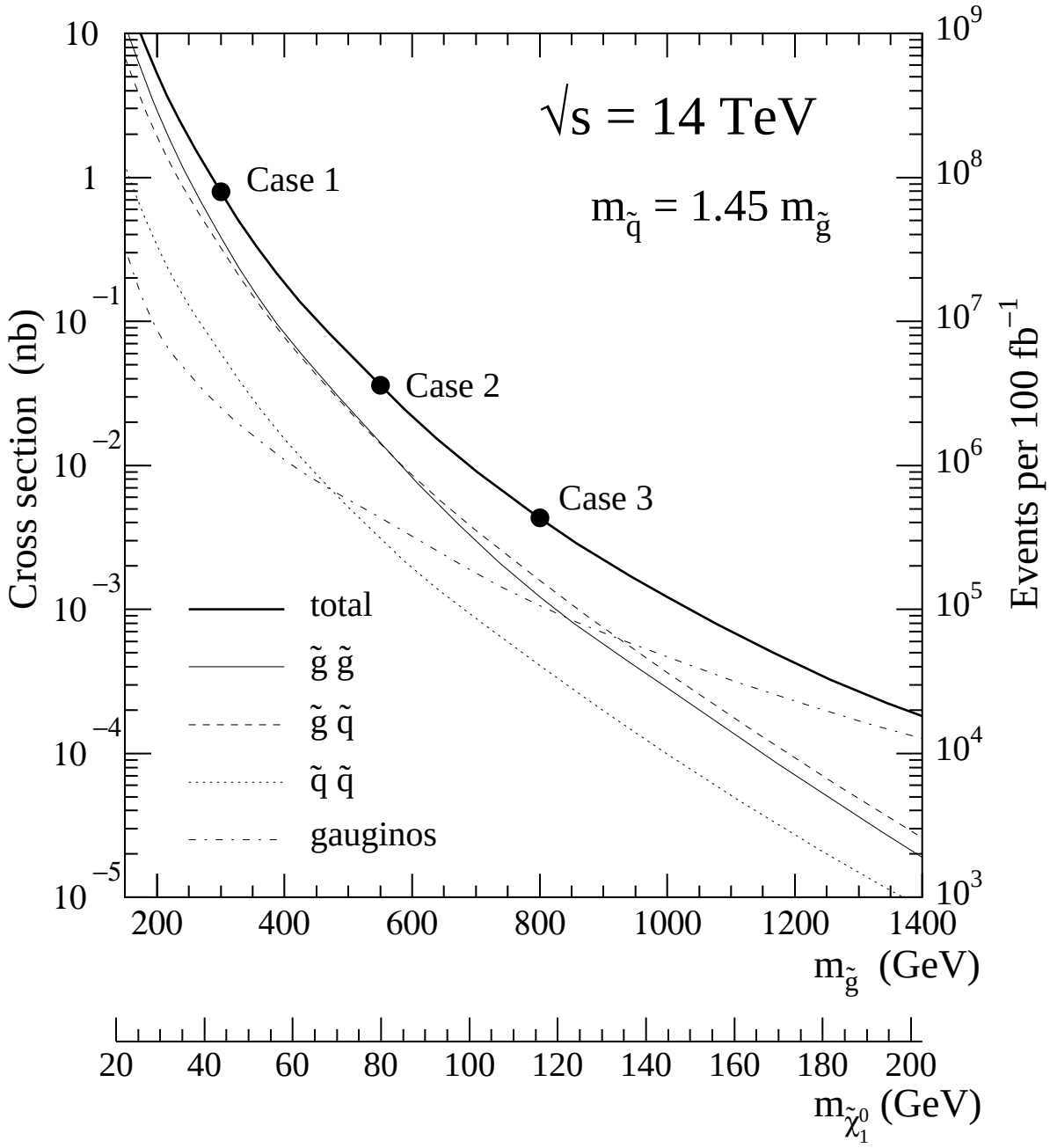

Figure 1: Total cross sections for the production of gluinos, squarks and gauginos in pp collisions at $\sqrt{s} = 14$ TeV as a function of the gluino mass $m_{\tilde{g}}$. The corresponding mass of the lightest neutralino $m_{\tilde{\chi}_1^0}$ is also shown. Also given in the vertical scale is the corresponding number of events per 100 fb^{-1}.

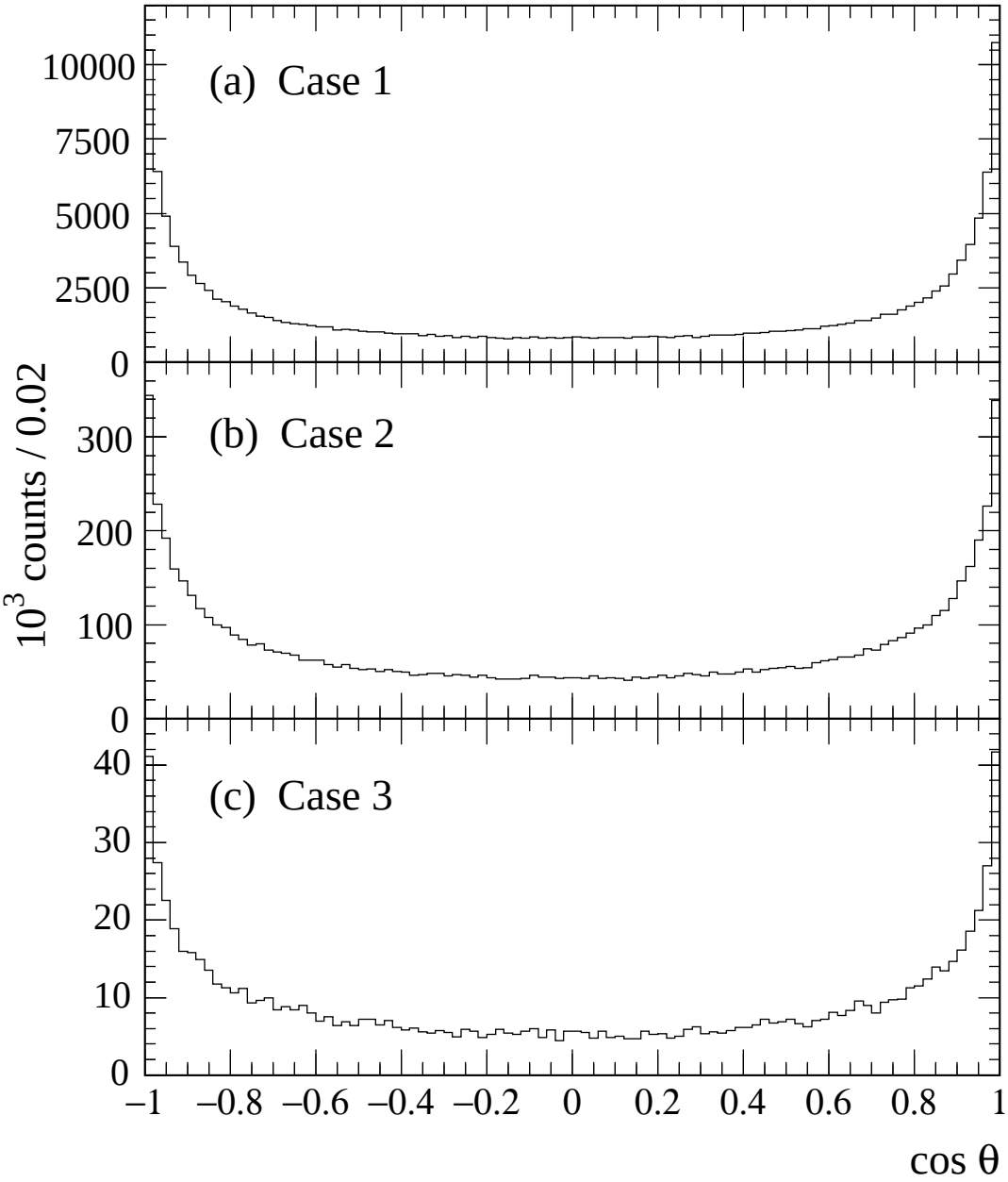

Figure 2: Angular distributions of $\tilde{\chi}_1^0$'s produced at the LHC with 100 fb^{-1} for (a) Case 1, (b) Case 2, and (c) Case 3.

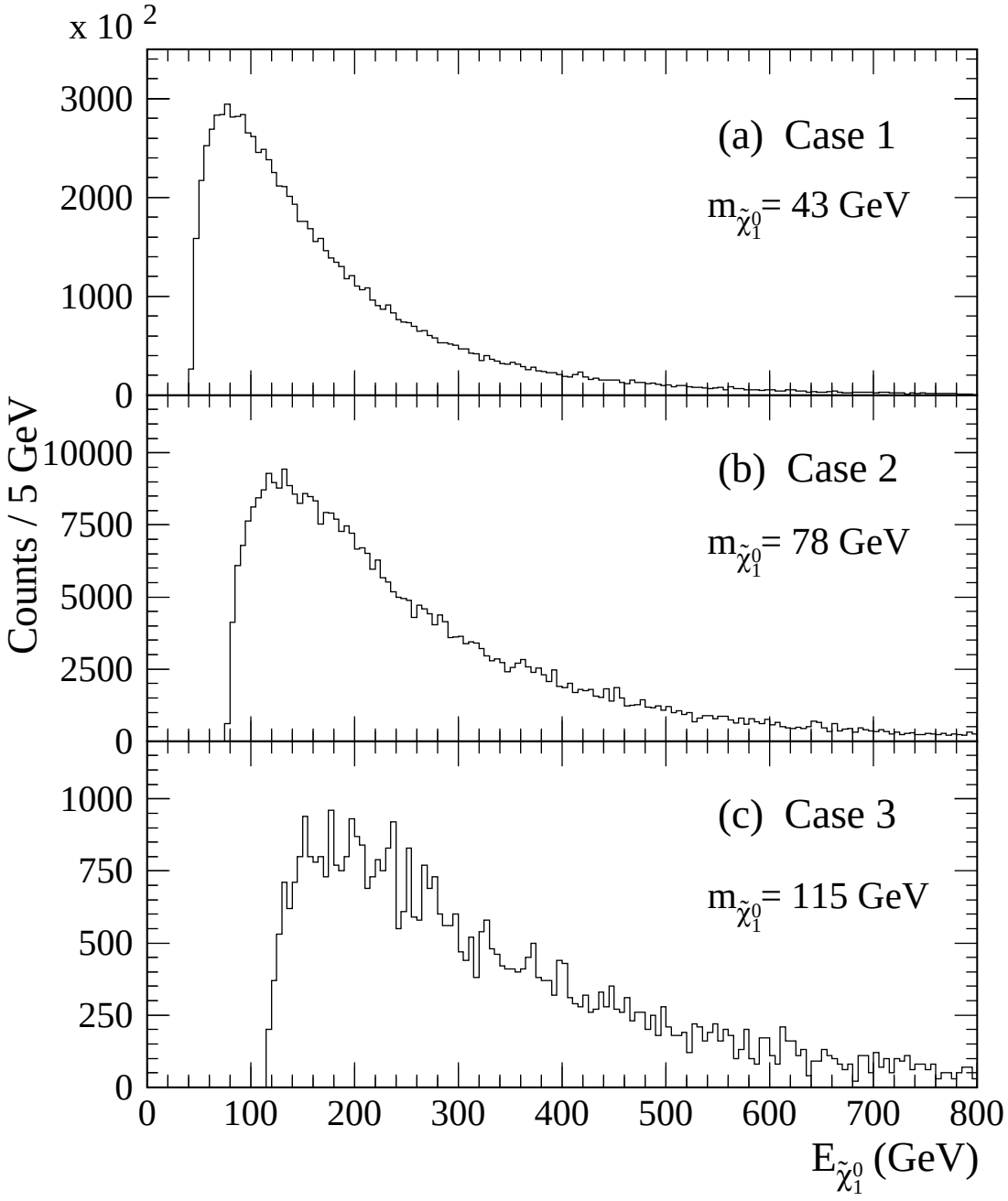

Figure 3: The energy spectra of $\tilde{\chi}_1^0$'s which point to the detector for (a) Case 1, (b) Case 2, and (c) Case 3.

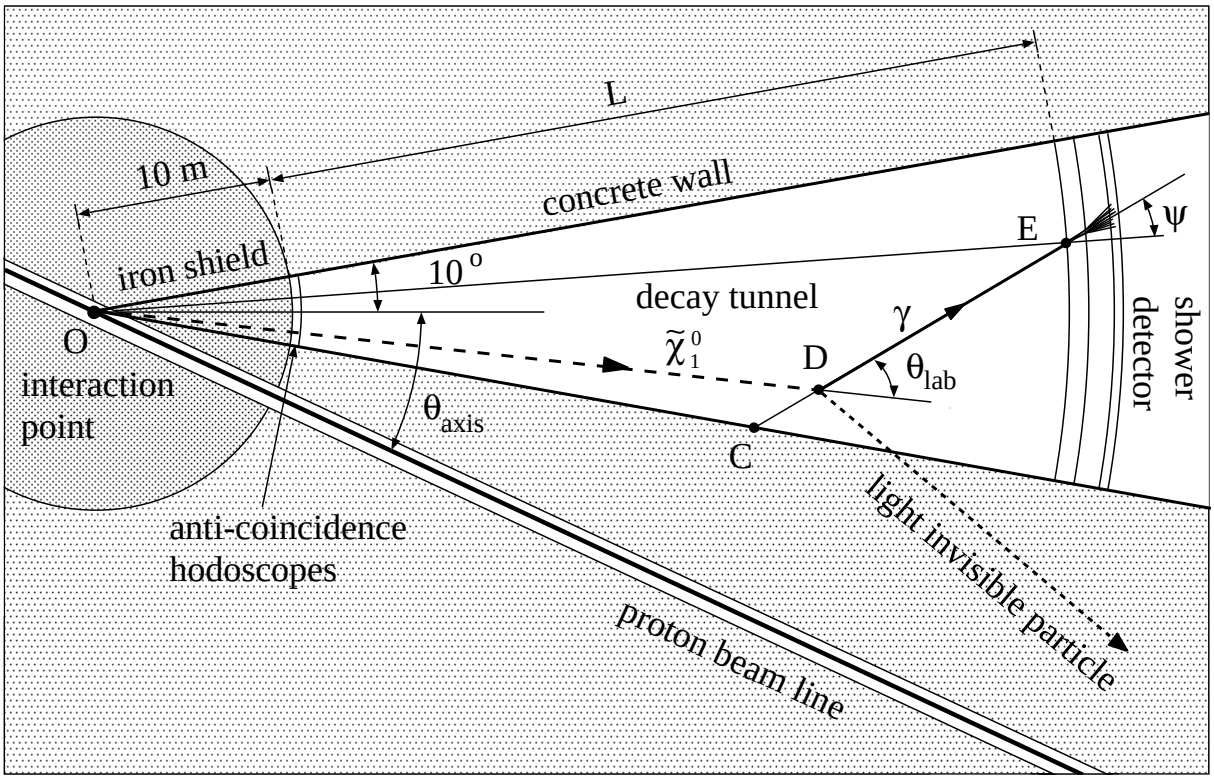

Figure 4: Schematic view of the setup. The lightest neutralino ($\tilde{\chi}_1^0$) is produced in pp collisions, goes through the iron shield, and decays in the tunnel to a photon (γ) plus a light invisible particle. The decay photon will then enter the shower detector, and be detected. An "active" 4π-shield consisting of segmented calorimeters, magnetized iron plates and the muon trackers can also be used instead of the bulk iron shield.

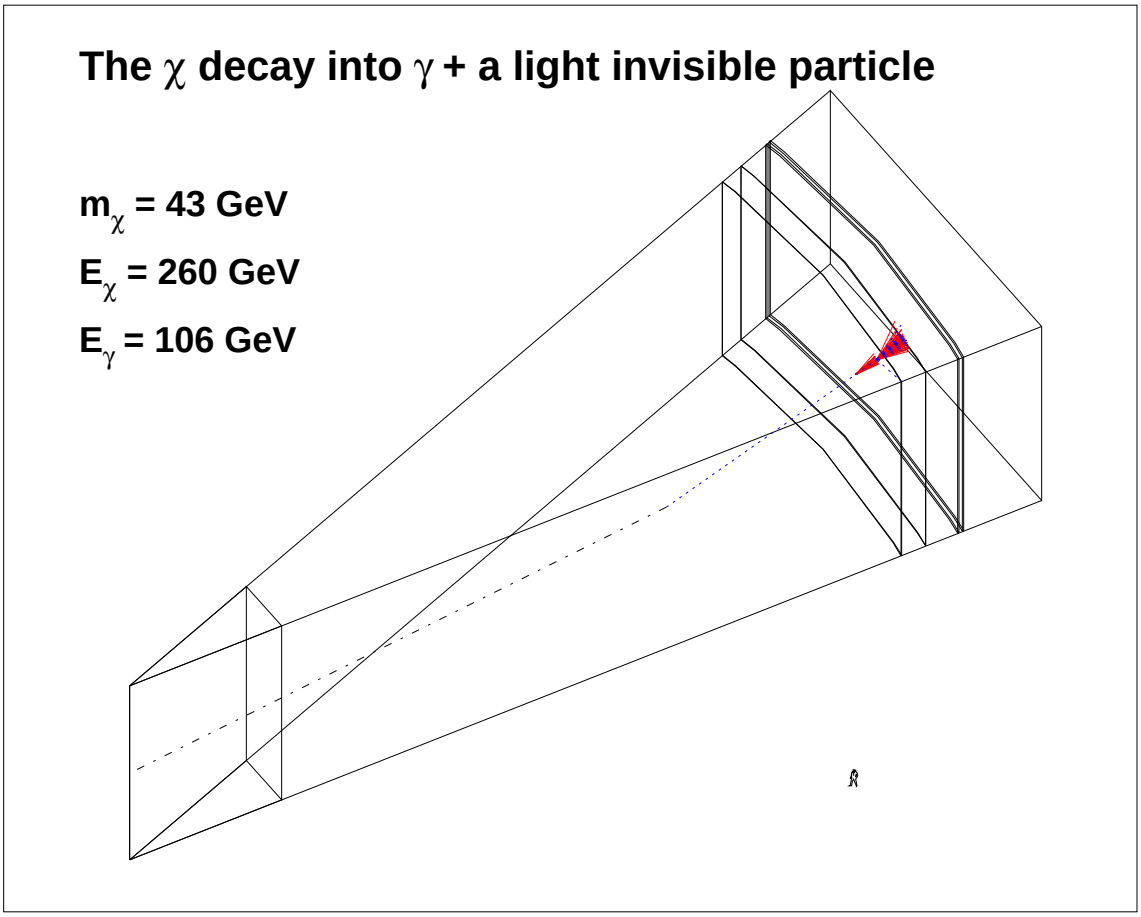

Figure 5: An example of the simulated $\tilde{\chi}_1^0$ decay into a photon and a light invisible particle. Dash-dotted, dotted and solid lines indicate tracks of the $\tilde{\chi}_1^0$, ≥ 50 MeV photons and electrons, respectively.

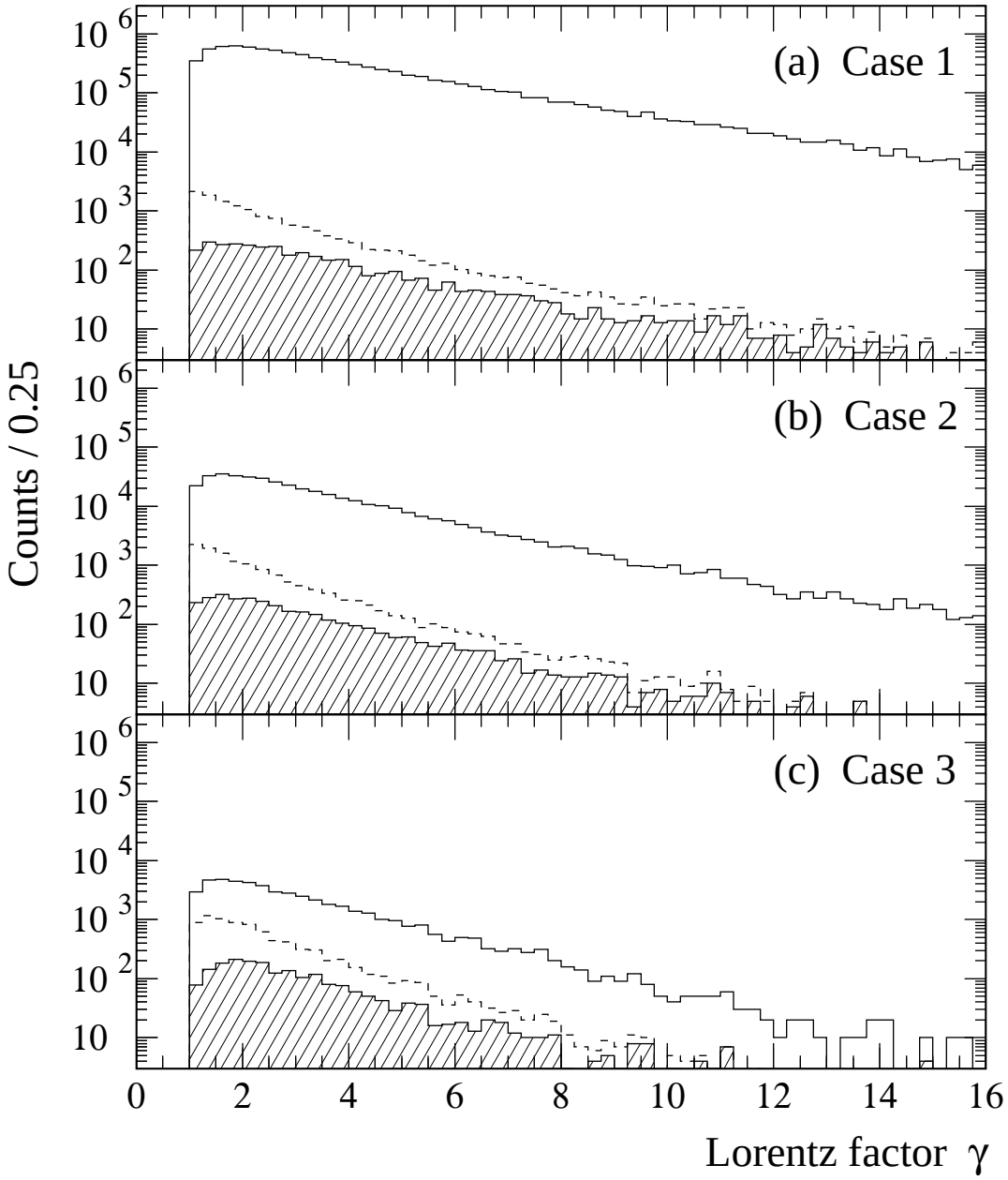

Figure 6: Lorentz factor (γ) distributions of $\tilde{\chi}_1^0$'s that enter (solid lines) or decay in (dashed lines) the decay tunnel for (a) Case 1, (b) Case 2, and (c) Case 3. Hatched histograms are for $\tilde{\chi}_1^0$'s whose decay photons enter the shower detector.

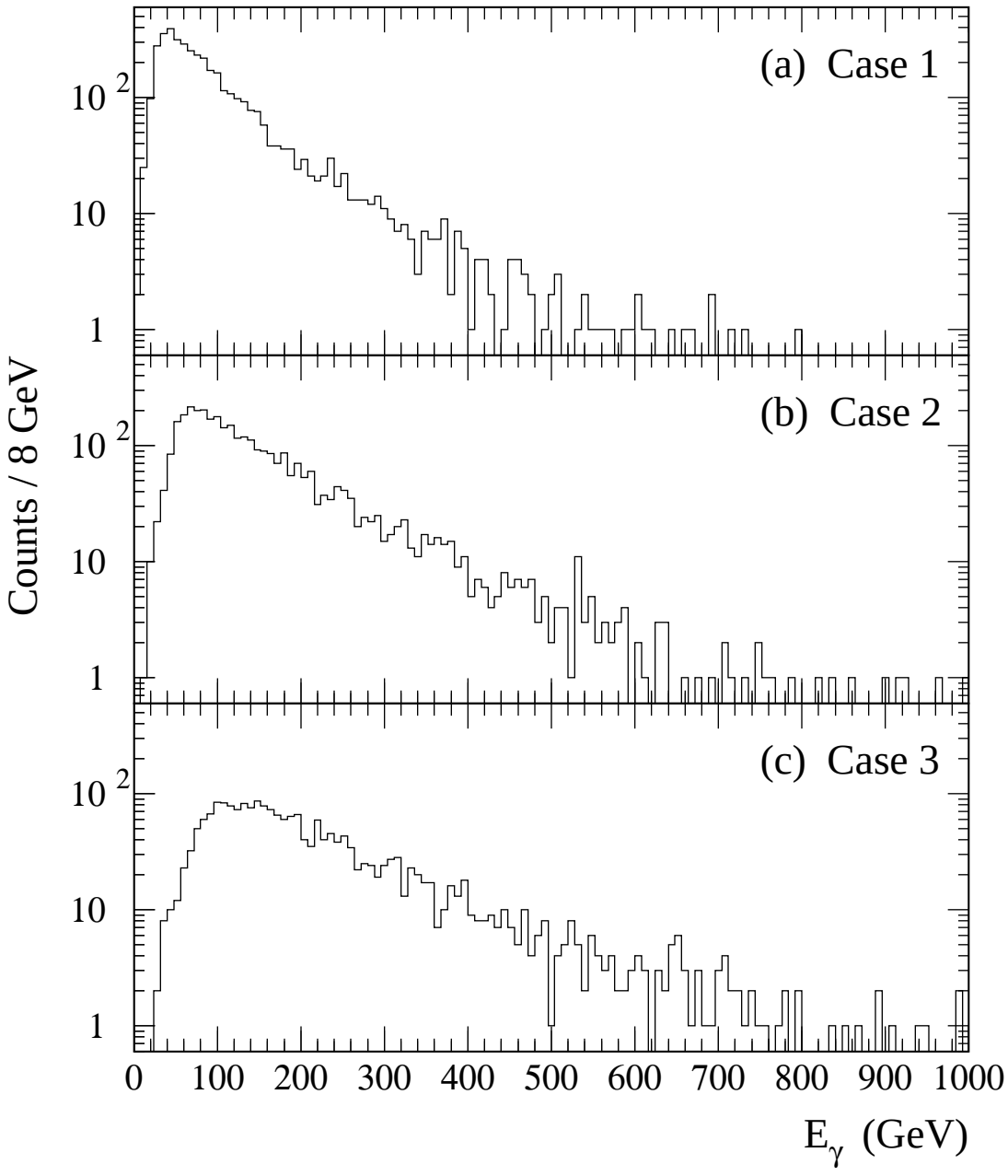

Figure 7: The energy spectra of the decay photons that enter the shower detector for (a) Case 1, (b) Case 2, and (c) Case 3.

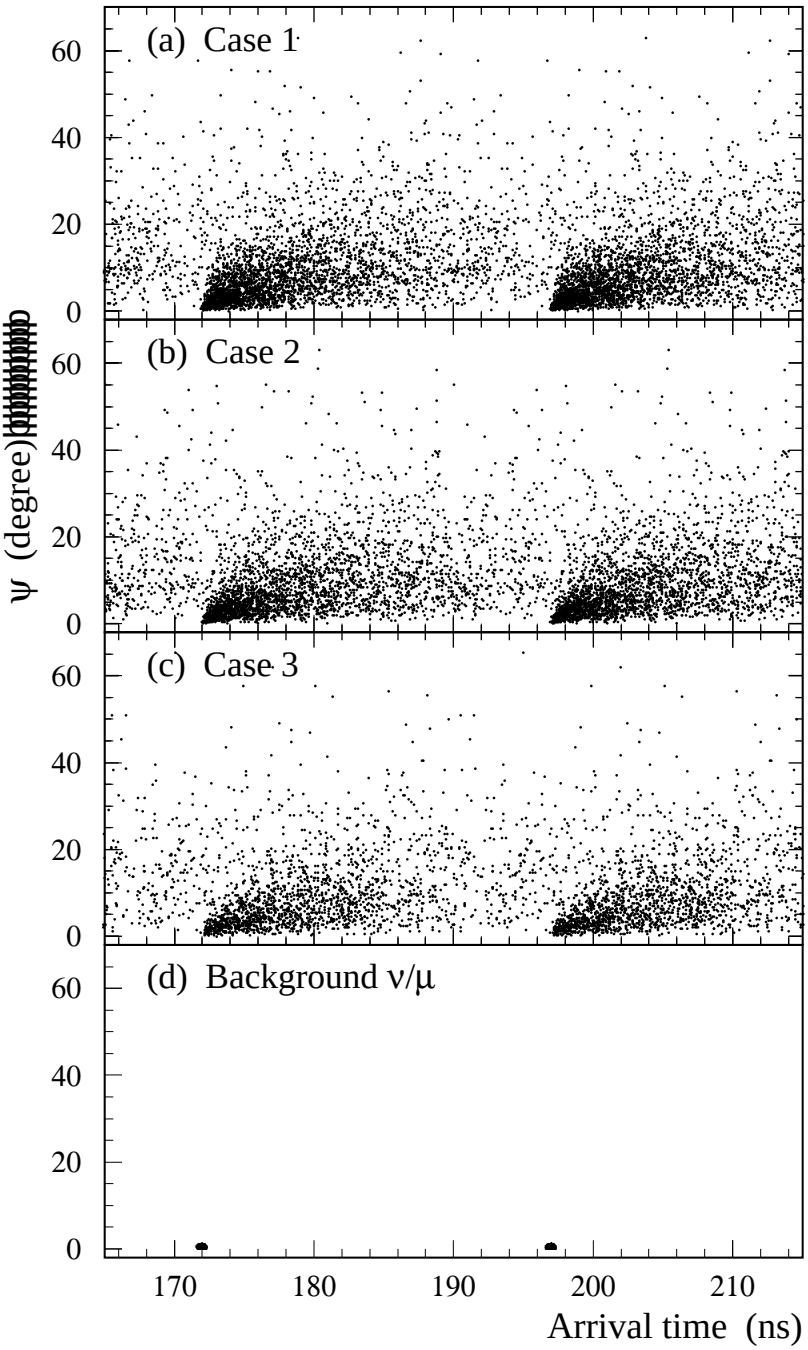

Figure 8: Scatter plots (ψ vs. the arrival time) of detected events for (a) Case 1, (b) Case 2, (c) Case 3, and (d) background neutrinos and muons. The resolutions of ψ and time measurements are assumed to be $\sigma_\psi = 0.3^\circ$ and $\sigma_t = 0.2$ ns, respectively.

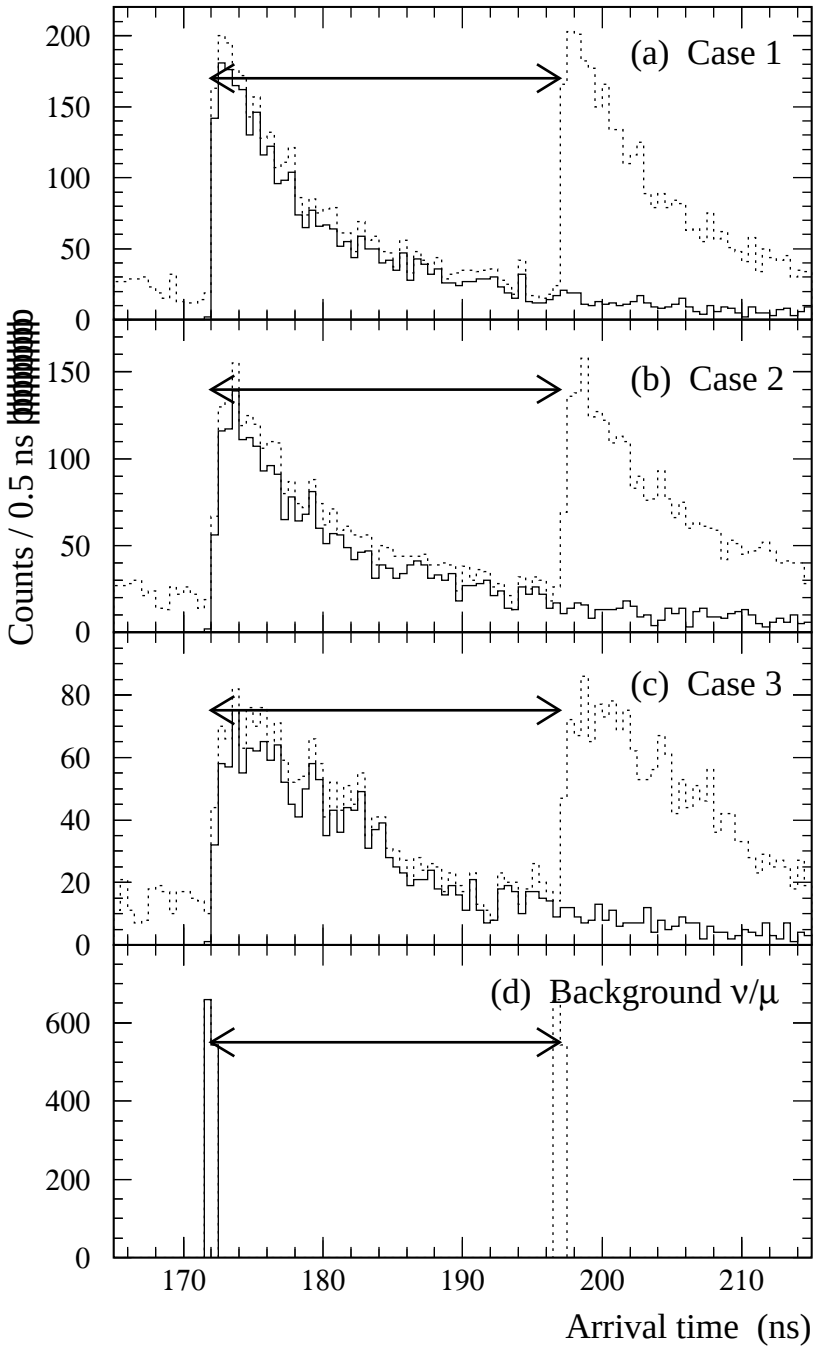

Figure 9: Distributions of the arrival time before (solid lines) and after (dotted lines) the bunch convolution for (a) Case 1, (b) Case 2, (c) Case 3, and (d) background neutrinos and muons. Arrows indicate the bunch spacing of 25 ns.

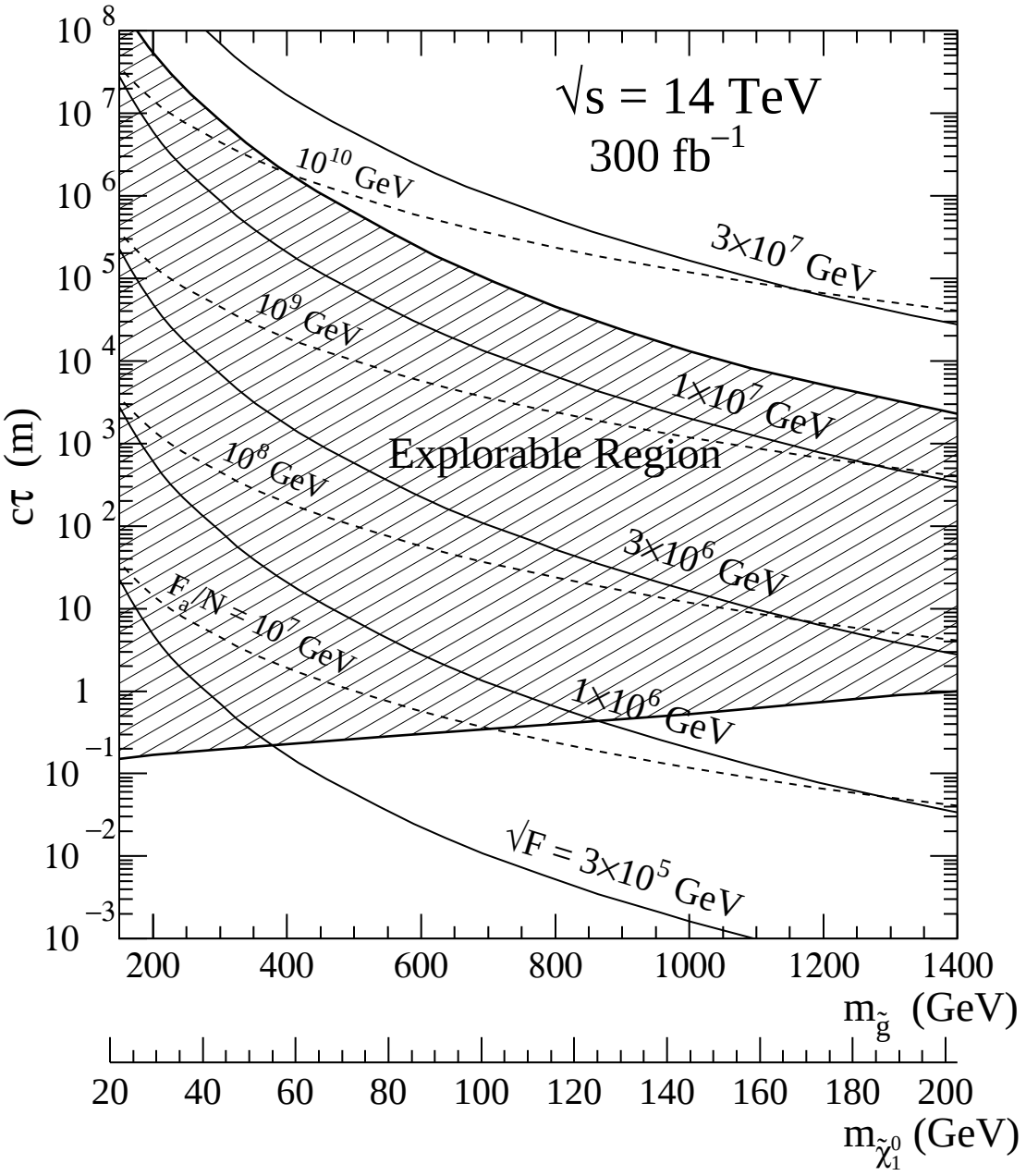

Figure 10: Explorable range of $c\tau$ for the $\tilde{\chi}_1^0$ decay at the LHC with 300 fb^{-1}. Also shown are the predicted curves of $c\tau(\tilde{\chi}_1^0 \to \gamma\tilde{G})$ for $\sqrt{F} = 3 \times 10^5$ to 3×10^7 GeV (solid lines) and $c\tau(\tilde{\chi}_1^0 \to \gamma\tilde{a})$ for $F_a/N = 10^7$ to 10^{10} GeV (dashed lines).

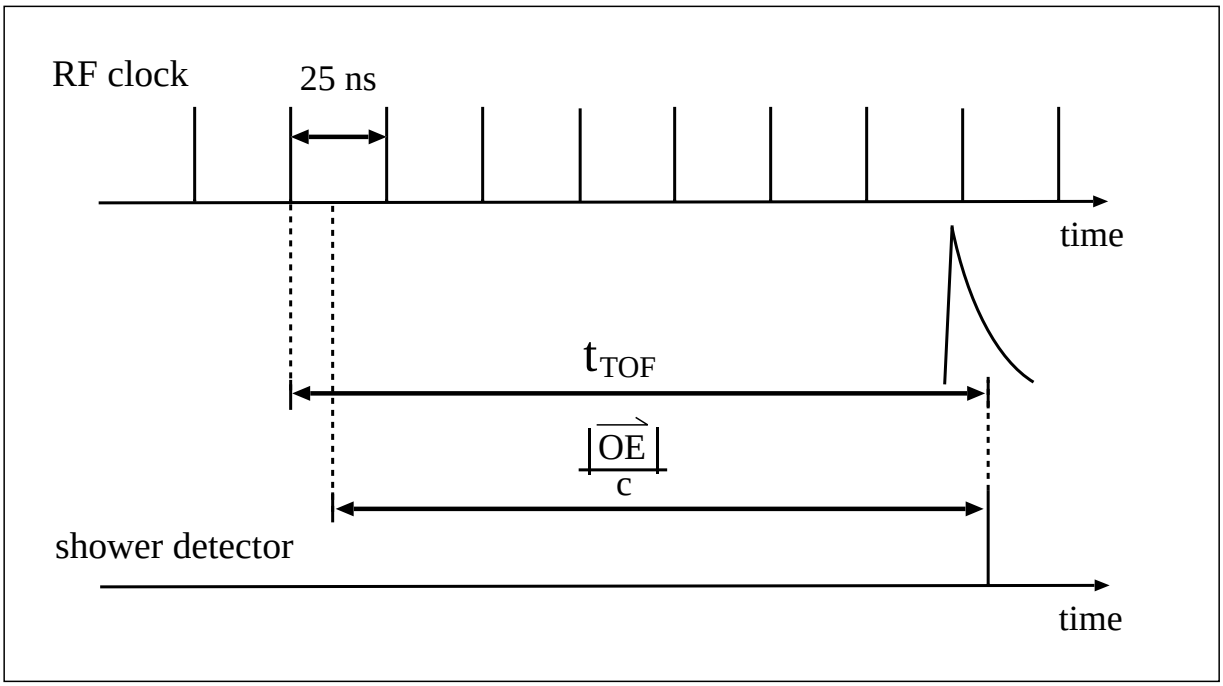

Figure 11: Timing chart of the $\tilde{\chi}_1^0$ decay event. The approximate time-of-flight (TOF) of $\tilde{\chi}_1^0$, $t_{\rm TOF}$, is extracted from the time difference between the signal of the shower detector and the RF pulse. Note that $|\overrightarrow{\rm OE}|/c$ is the minimum possible TOF on the condition of $\beta \leq 1$.

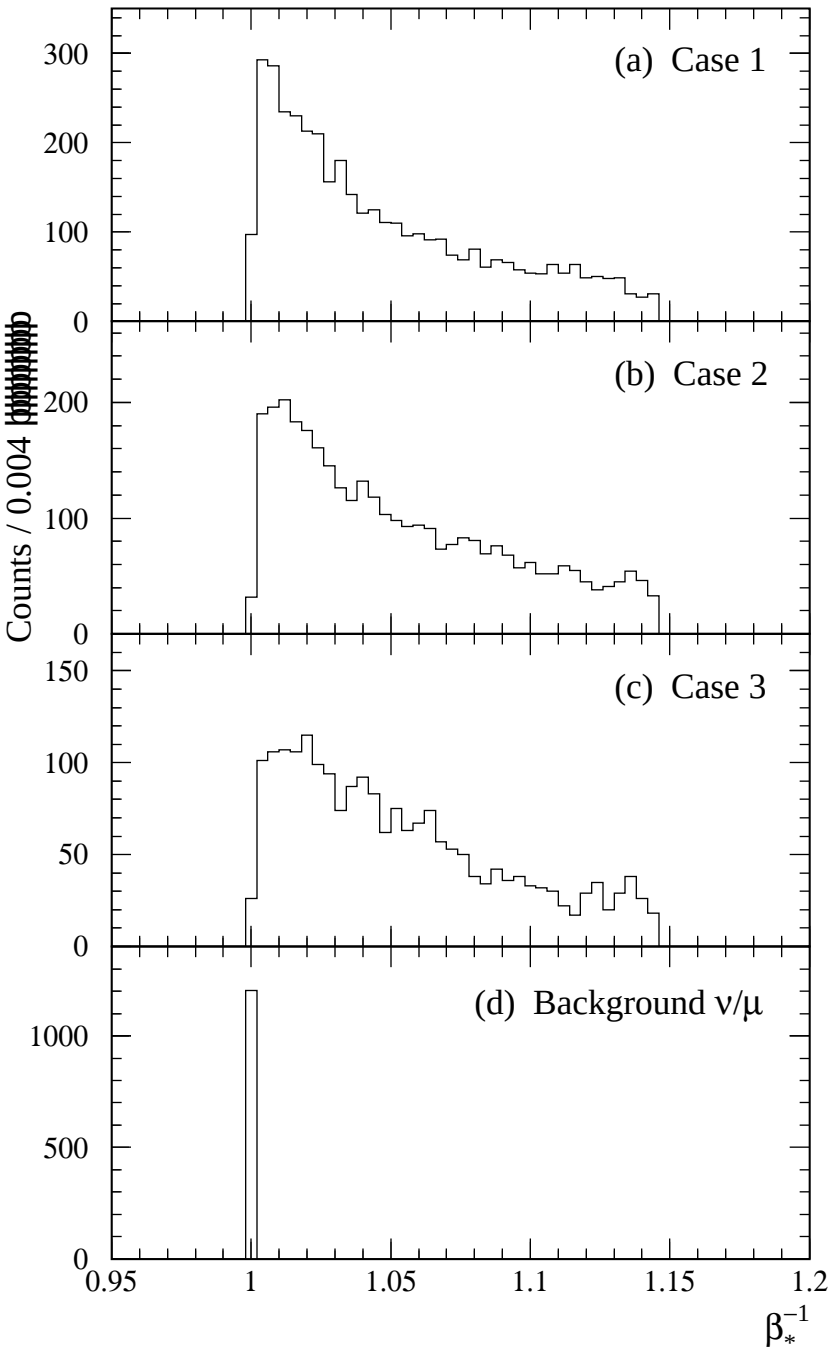

Figure 12: Distributions of β_*^{-1} for (a) Case 1, (b) Case 2, (c) Case 3, and (d) background neutrinos and muons.

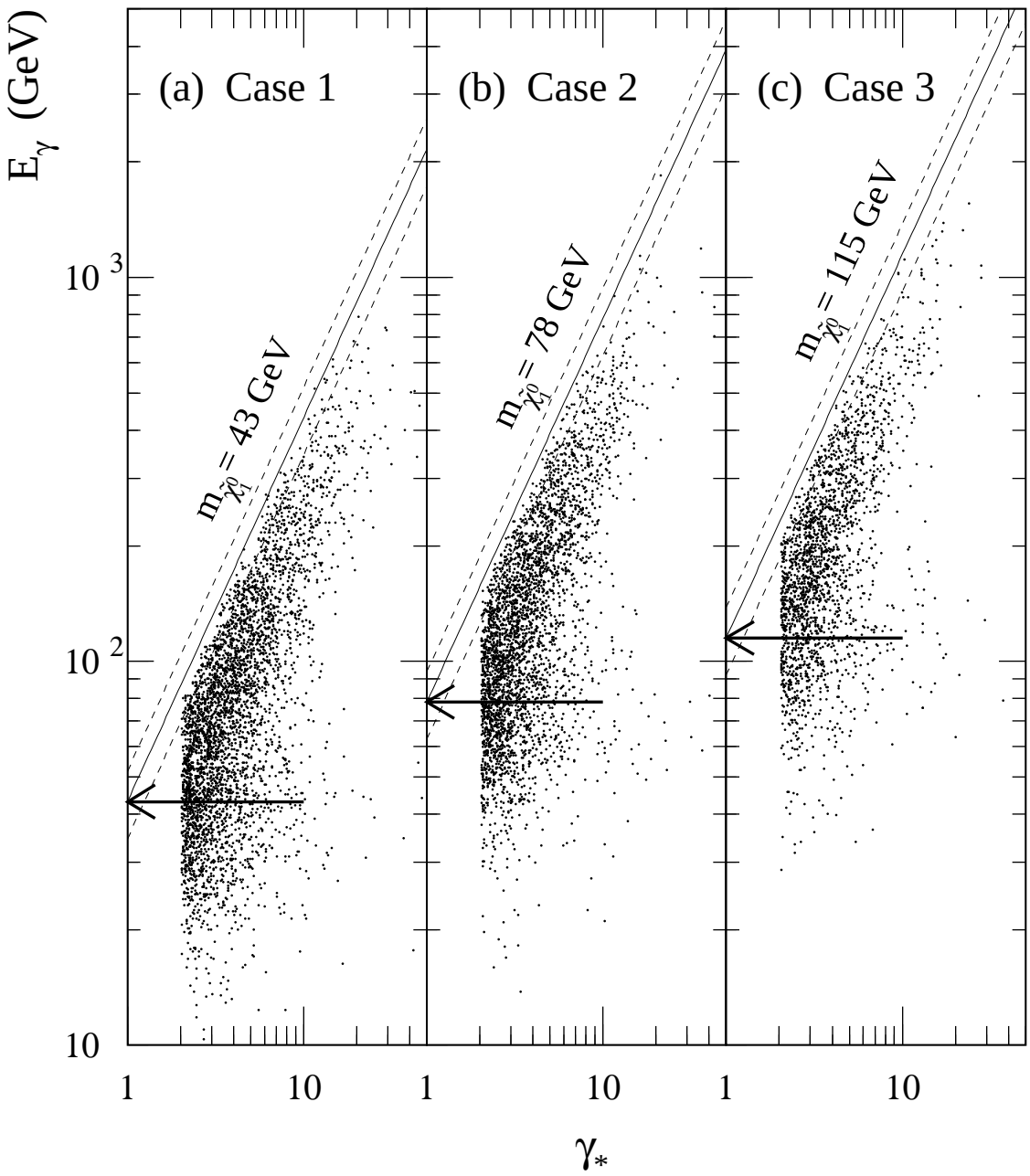

Figure 13: Scatter plots of E_γ vs. γ_* for (a) Case 1, (b) Case 2, and (c) Case 3. The solid lines correspond to $E_\gamma = m_{\tilde{\chi}_1^0}\gamma_*$, and the dashed lines are for $m_{\tilde{\chi}_1^0}$ deviated from the true value by $\pm 20\%$.

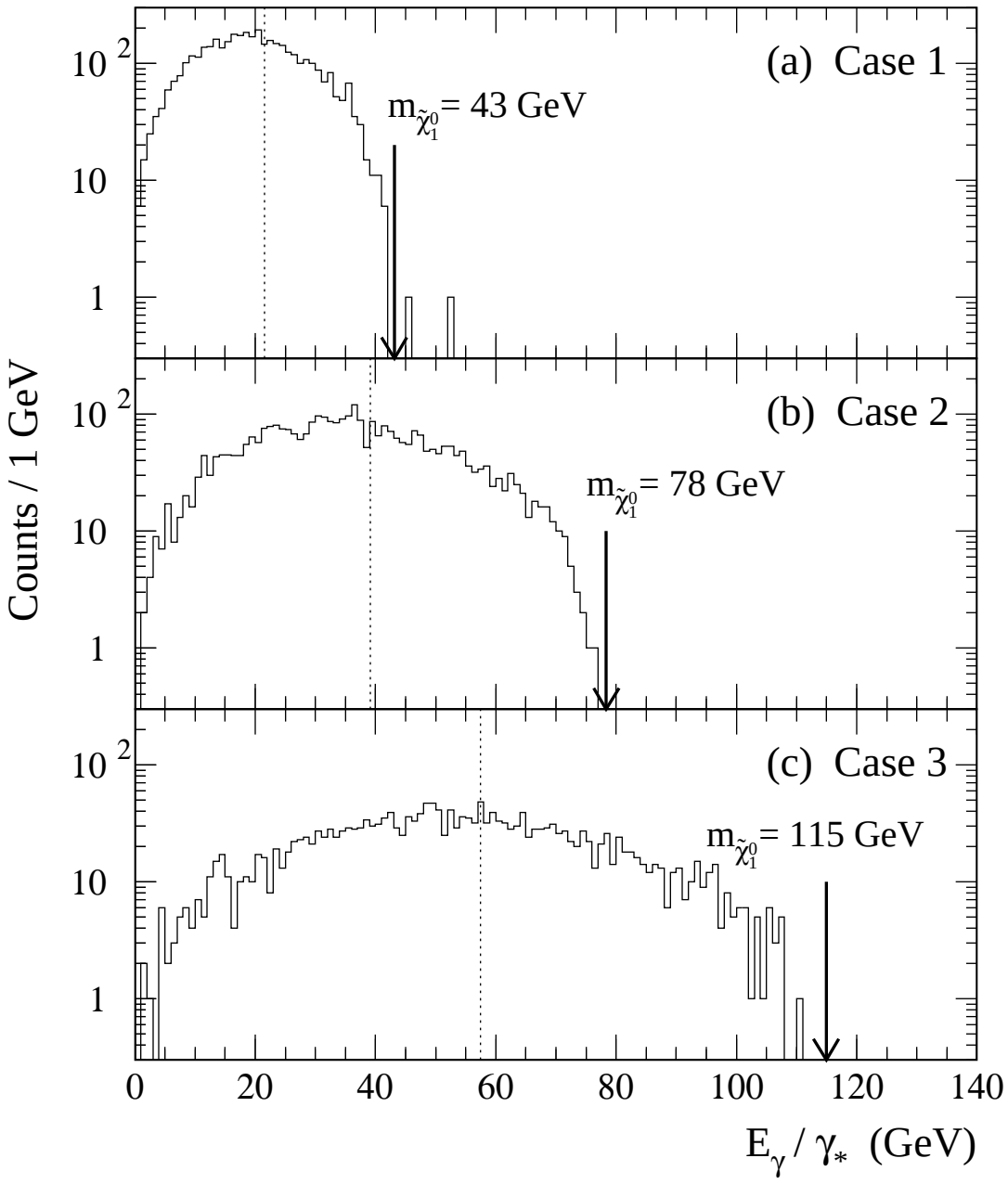

Figure 14: Distributions of E_γ/γ_* for (a) Case 1, (b) Case 2, and (c) Case 3. Arrows indicate the position of $E_\gamma/\gamma_* = m_{\tilde{\chi}_1^0}$. The dotted lines show the position of $E_\gamma/\gamma_* = m_{\tilde{\chi}_1^0}/2$.

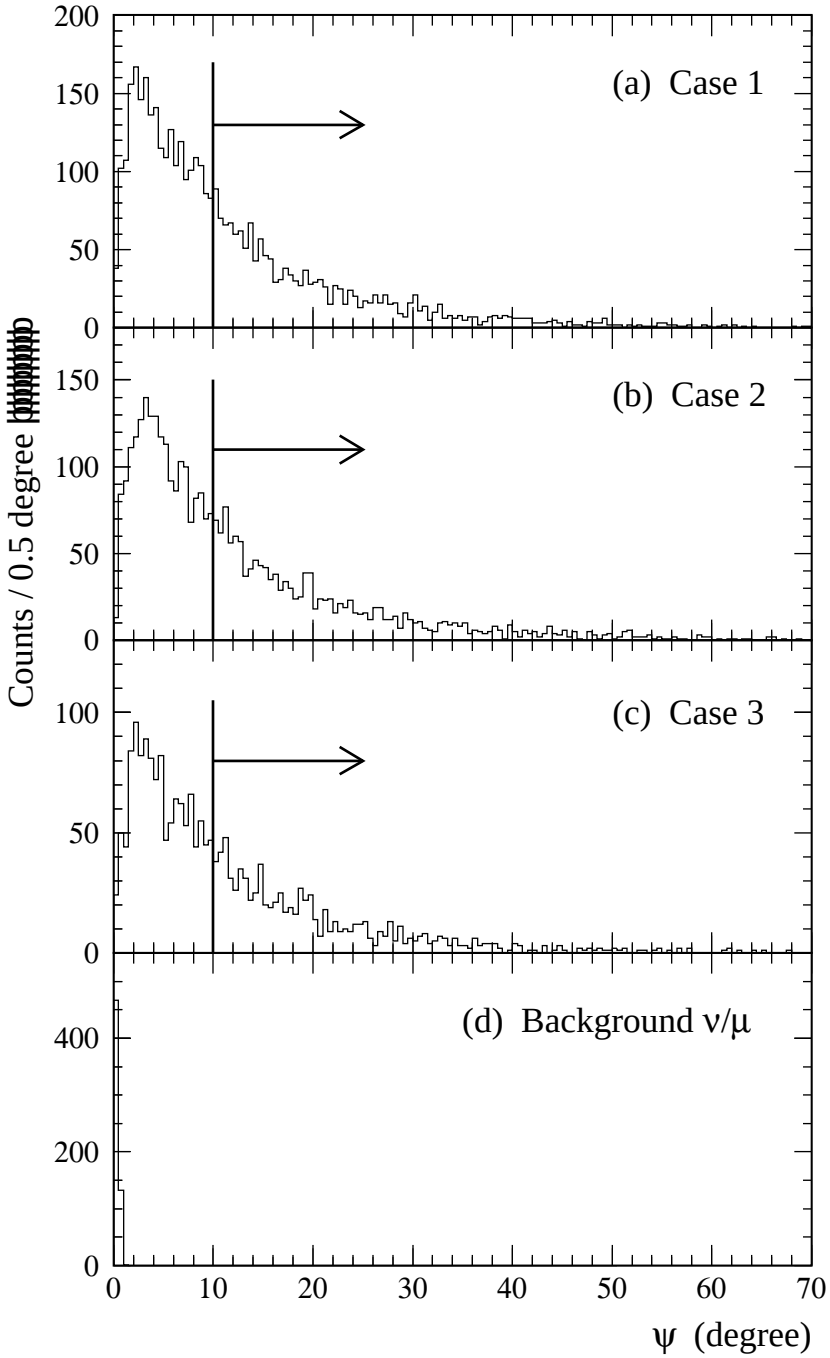

Figure 15: Distributions of the off angle ψ for (a) Case 1, (b) Case 2, (c) Case 3, and (d) background neutrinos and muons. The cut position for the kinematical analysis is also shown.

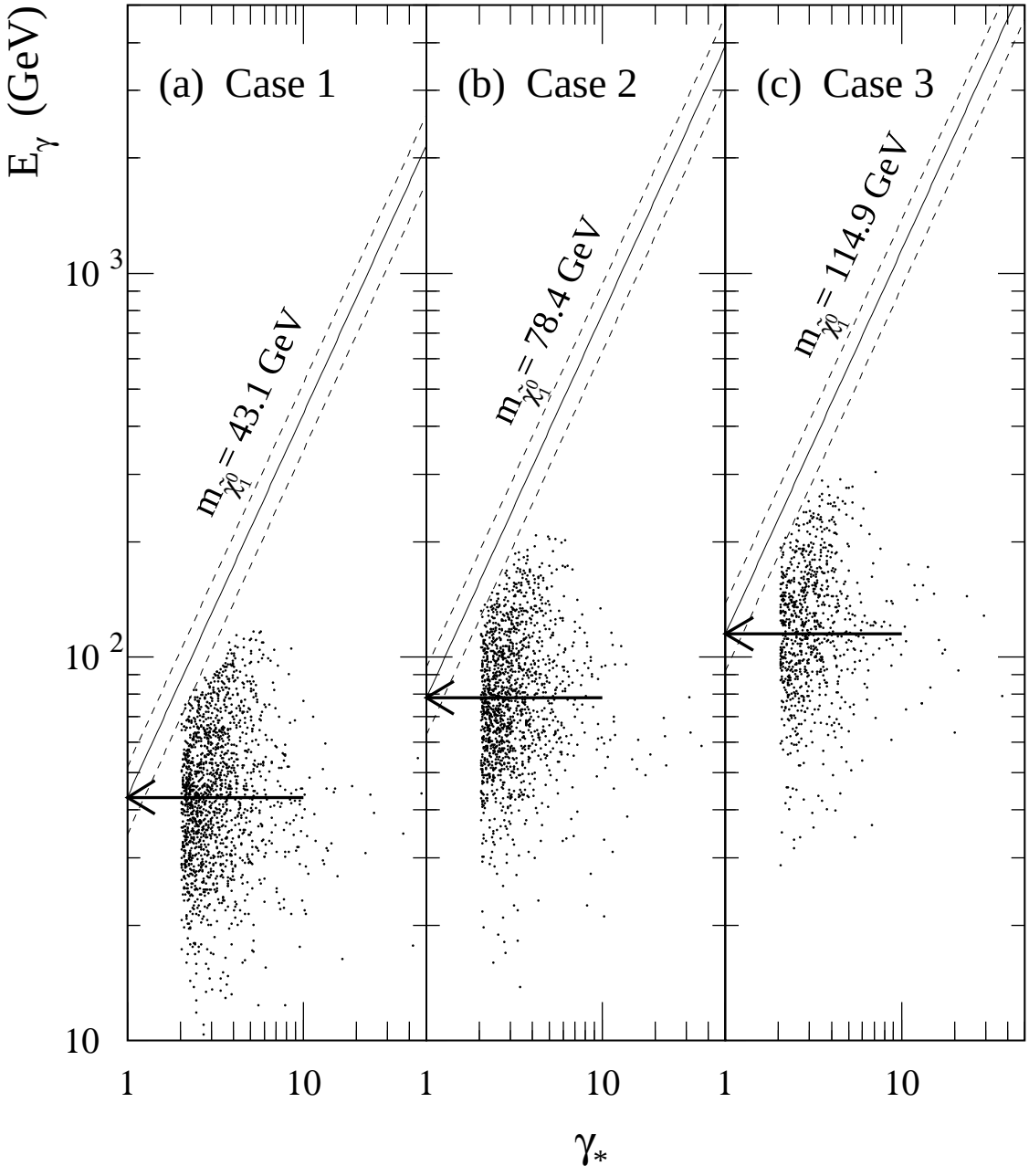

Figure 16: Same as Fig. 13 after applying the cut of $\psi \geq 10°$.

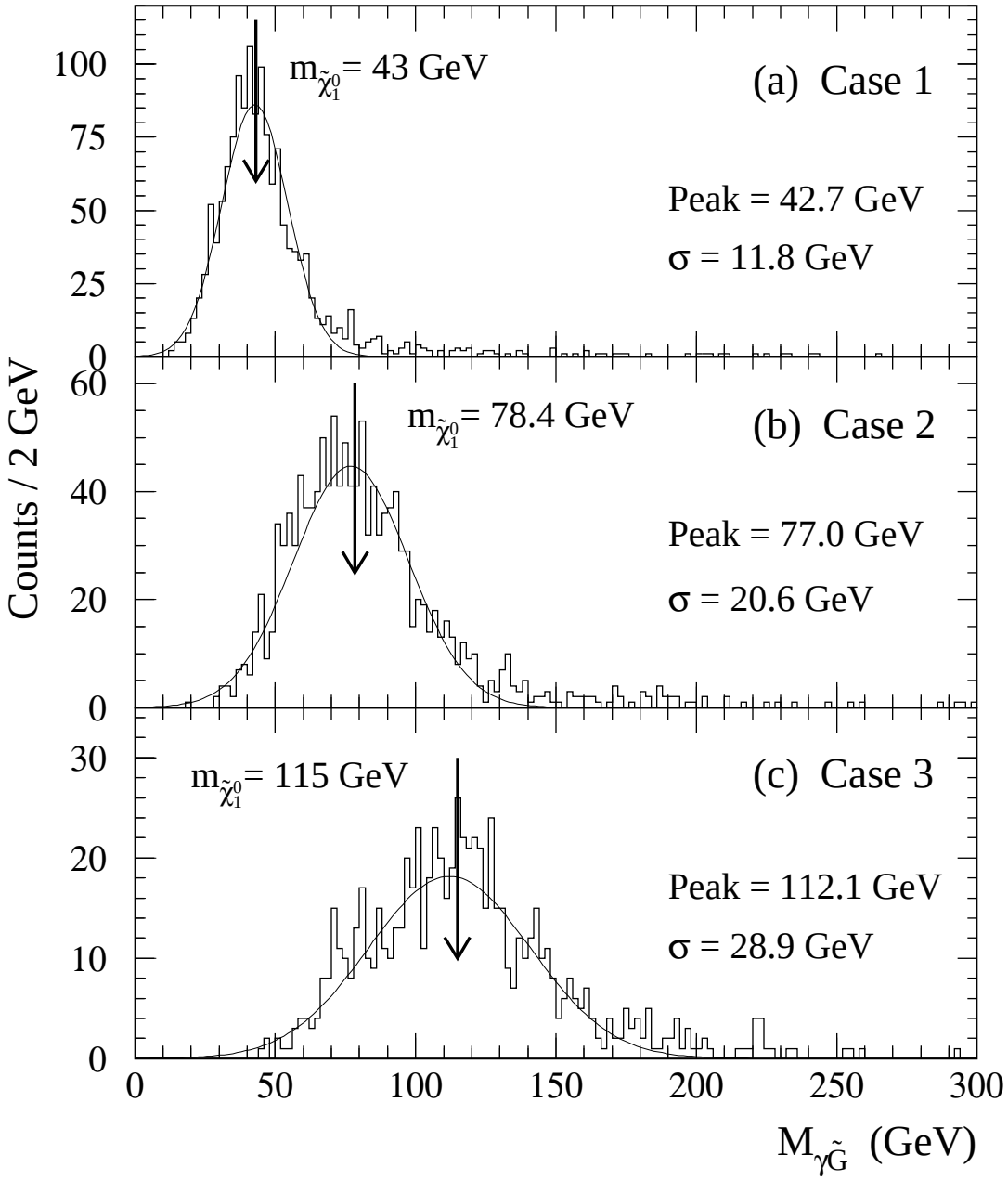

Figure 17: Distributions of the reconstructed mass $M_{\gamma\tilde{G}}$ for (a) Case 1, (b) Case 2, and (c) Case 3. Solid lines show the results of the fit by a gaussian. Arrows indicate the position of $M_{\gamma\tilde{G}} = m_{\tilde{\chi}_1^0}$.

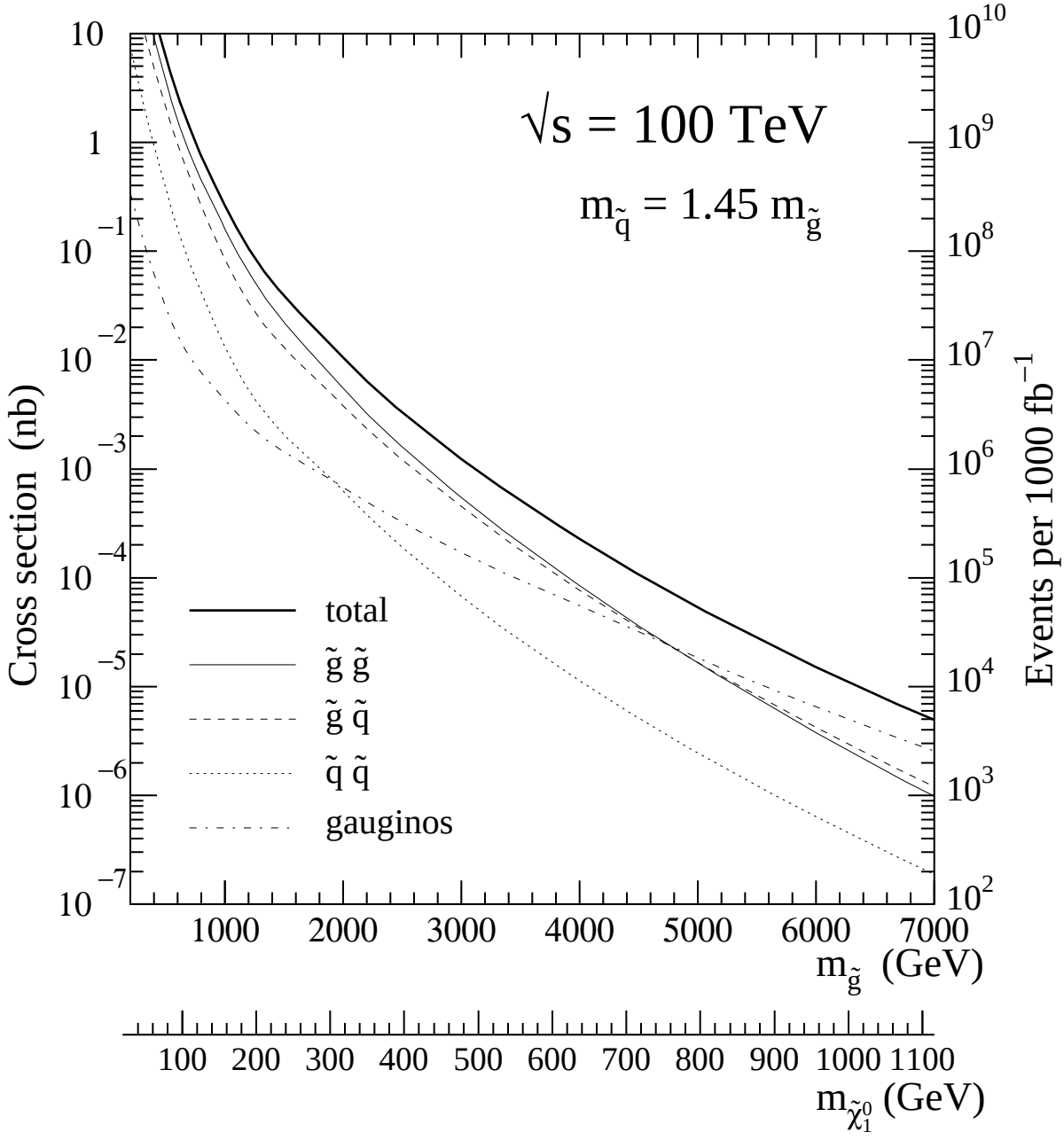

Figure 18: Total cross sections for the production of gluinos, squarks and gauginos in pp collisions at $\sqrt{s} = 100$ TeV as a function of $m_{\tilde{g}}$. The corresponding values of $m_{\tilde{\chi}_1^0}$ are also shown. Also given in the vertical scale is the corresponding number of events per 1000 fb^{-1}.

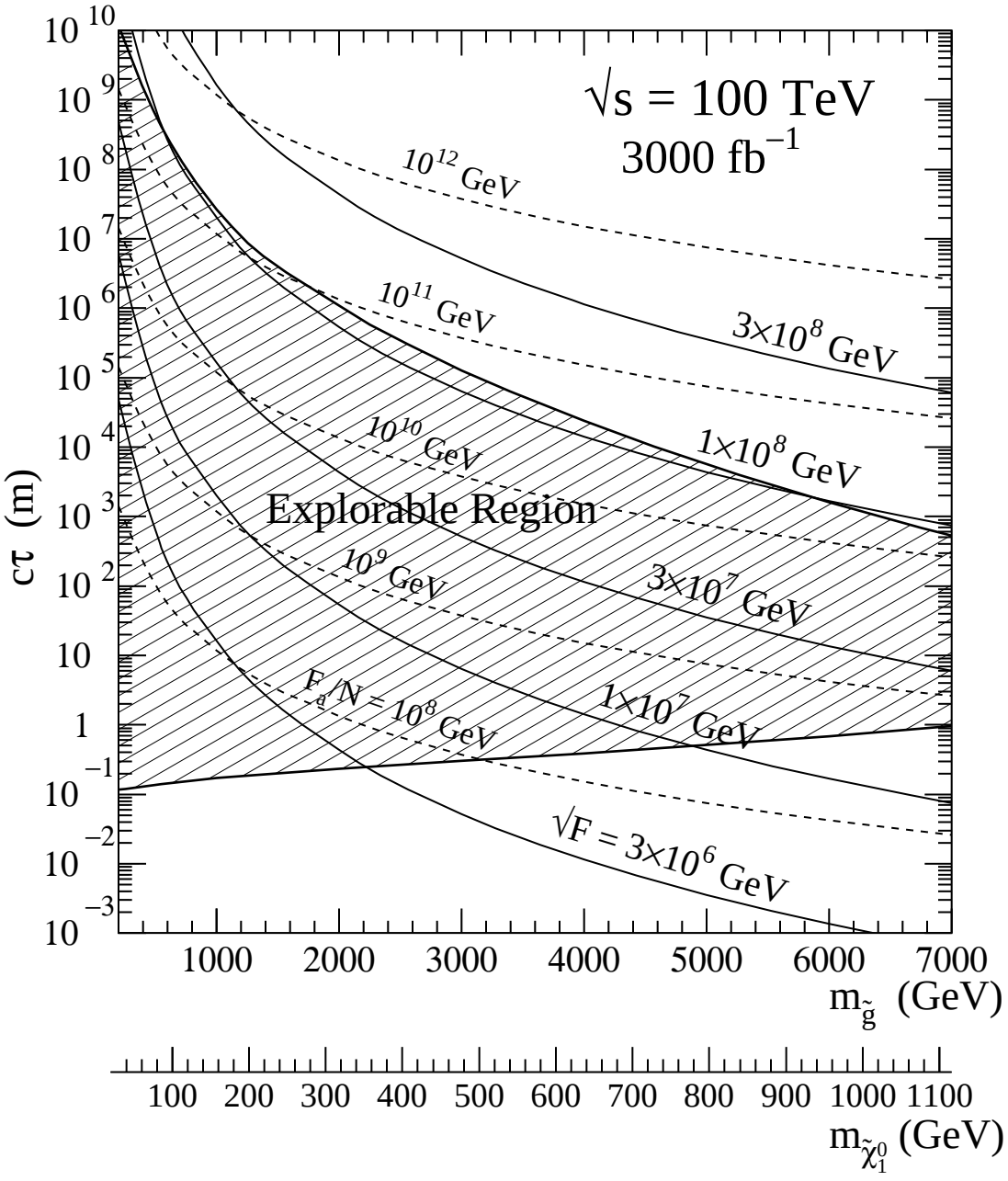

Figure 19: Explorable range of $c\tau$ for the $\tilde{\chi}_1^0$ decay at VLHC with 3000 fb^{-1}. Also shown are the predicted curves of $c\tau(\tilde{\chi}_1^0 \to \gamma\tilde{G})$ for $\sqrt{F} = 3 \times 10^6$ to 3×10^8 GeV (solid lines) and $c\tau(\tilde{\chi}_1^0 \to \gamma\tilde{a})$ for $F_a/N = 10^8$ to 10^{12} GeV (dashed lines).

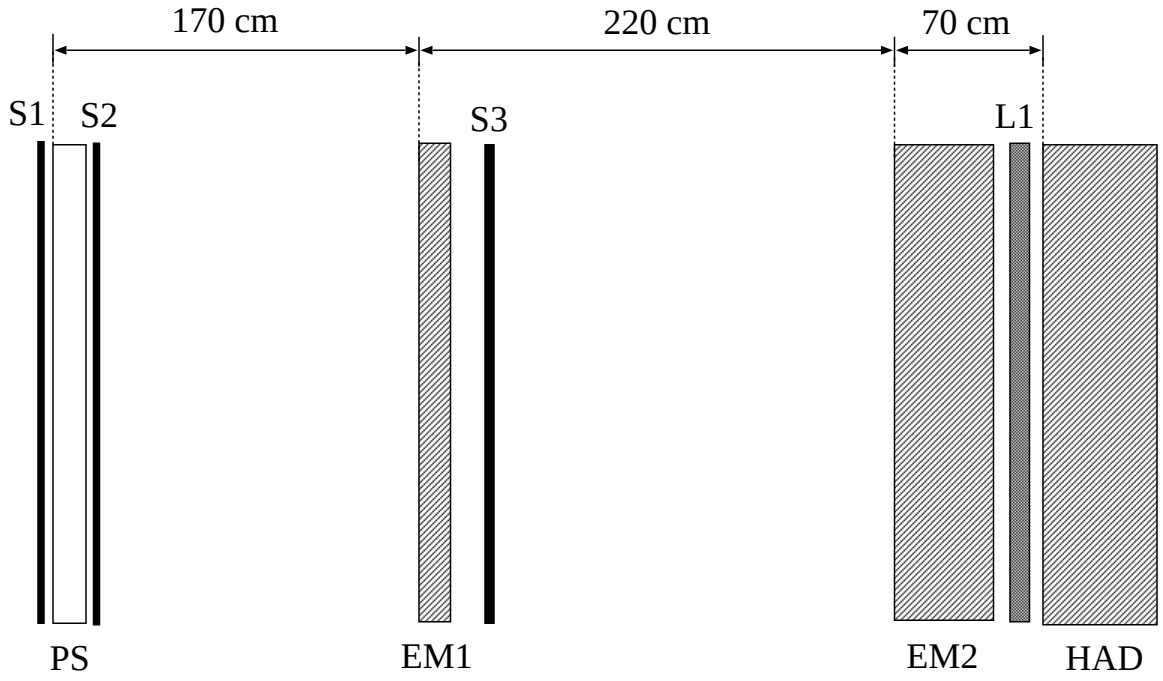

Figure 20: The schematic of the shower detector we investigated. It consists of the preshower detector (PS), two parts of the electromagnetic calorimeter (EM1 and EM2), three planes of plastic scintillators (S1, S2 and S3), the lead absorber (L1), and the hadron calorimeter (HAD).

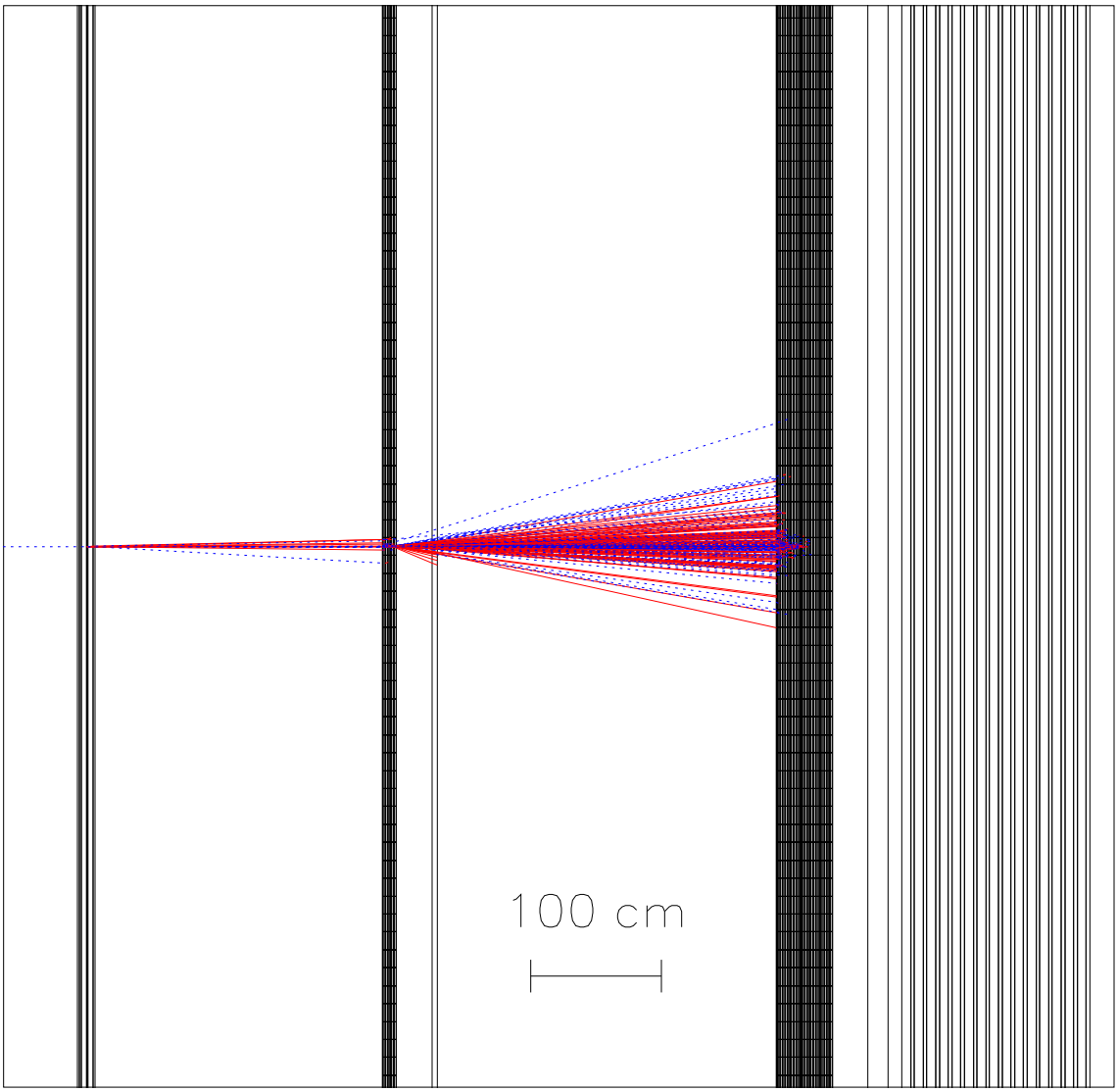

Figure 21: An example of the simulated electromagnetic shower which is initiated by 100 GeV photon incident on the shower detector. Solid and dashed lines indicate tracks of $\geq$ 50 MeV electrons and photons, respectively.

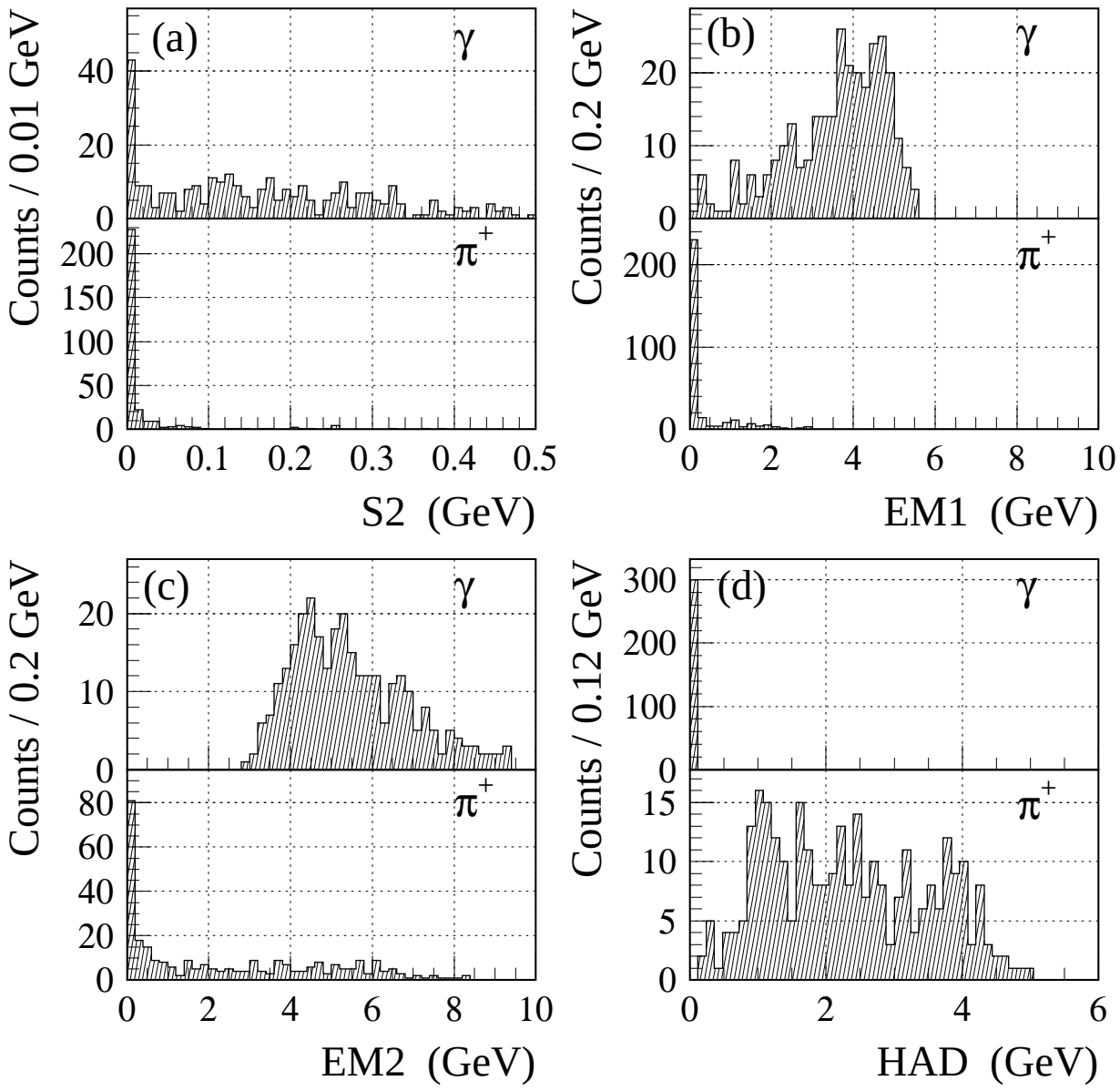

Figure 22: Distributions of energy deposited by 100 GeV photons and charged pions in (a) S2, (b) EM1, (c) EM2, and (d) HAD.

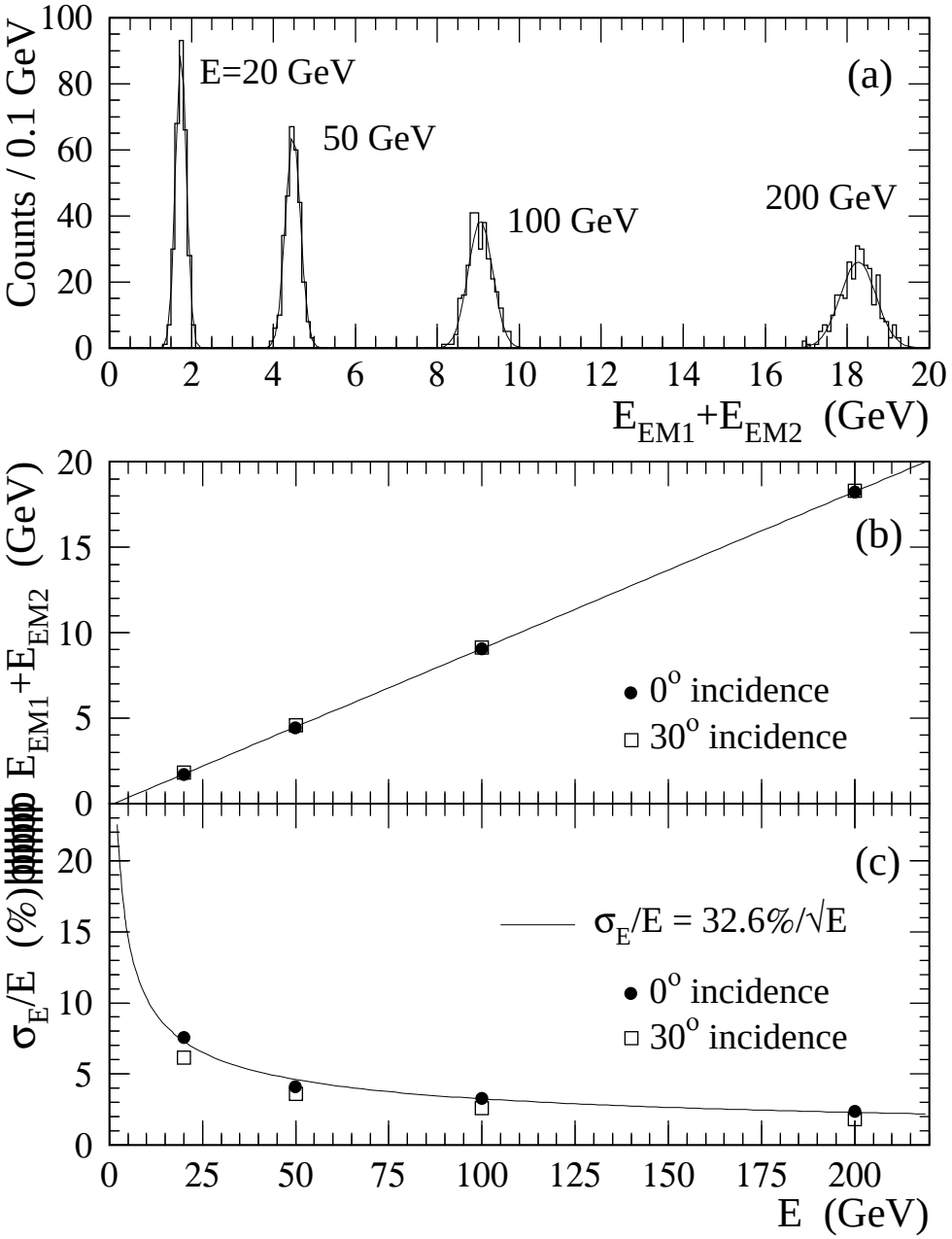

Figure 23: (a) Distributions of the sum of deposit energy in EM1 and EM2 for photons incident at 0° on the shower detector with energy E = 20, 50, 100 and 200 GeV. The results of the fit by a gaussian are also shown. (b) The sum of deposit energy in EM1 and EM2 vs. incident photon energy. (c) The energy resolution as a function of incident photon energy. The curve is the result of the fit for 0° data.

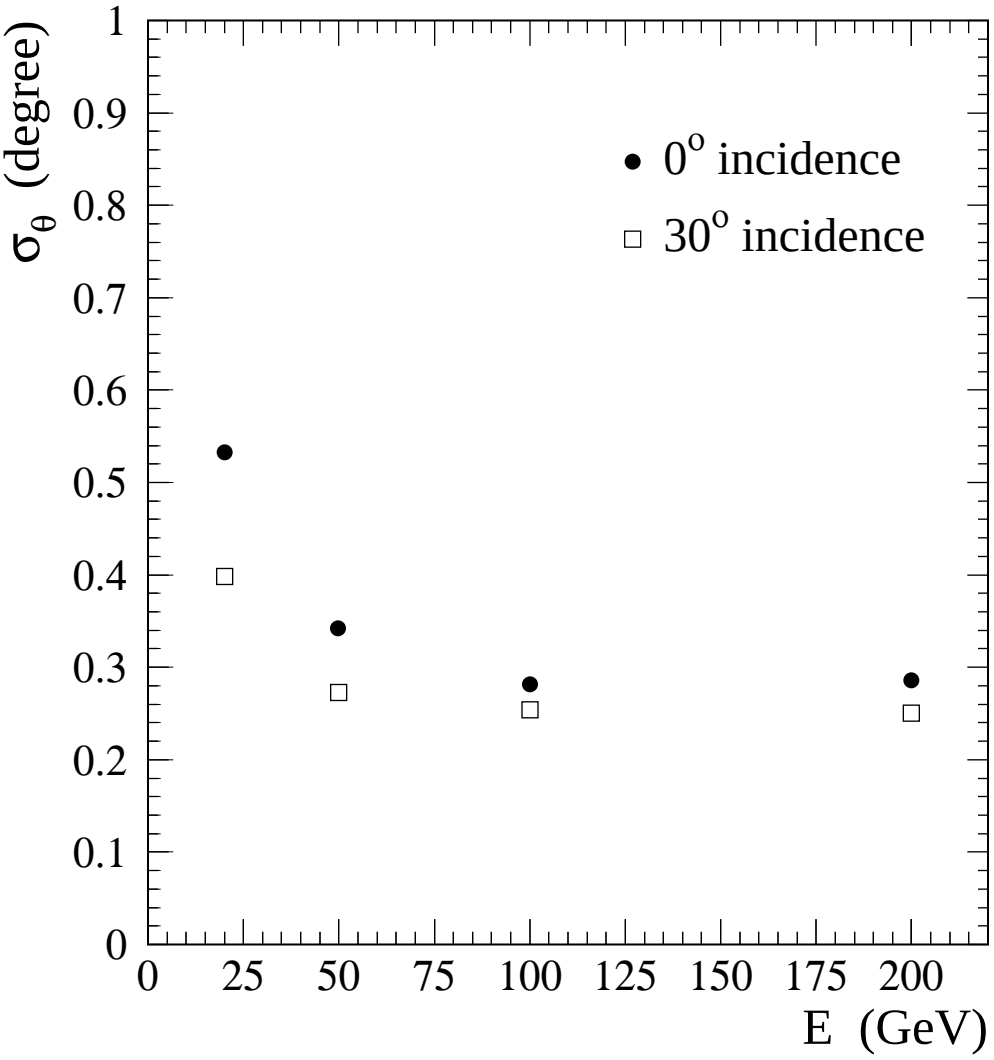

Figure 24: The angular resolution of the reconstructed shower direction as a function of incident photon energy.

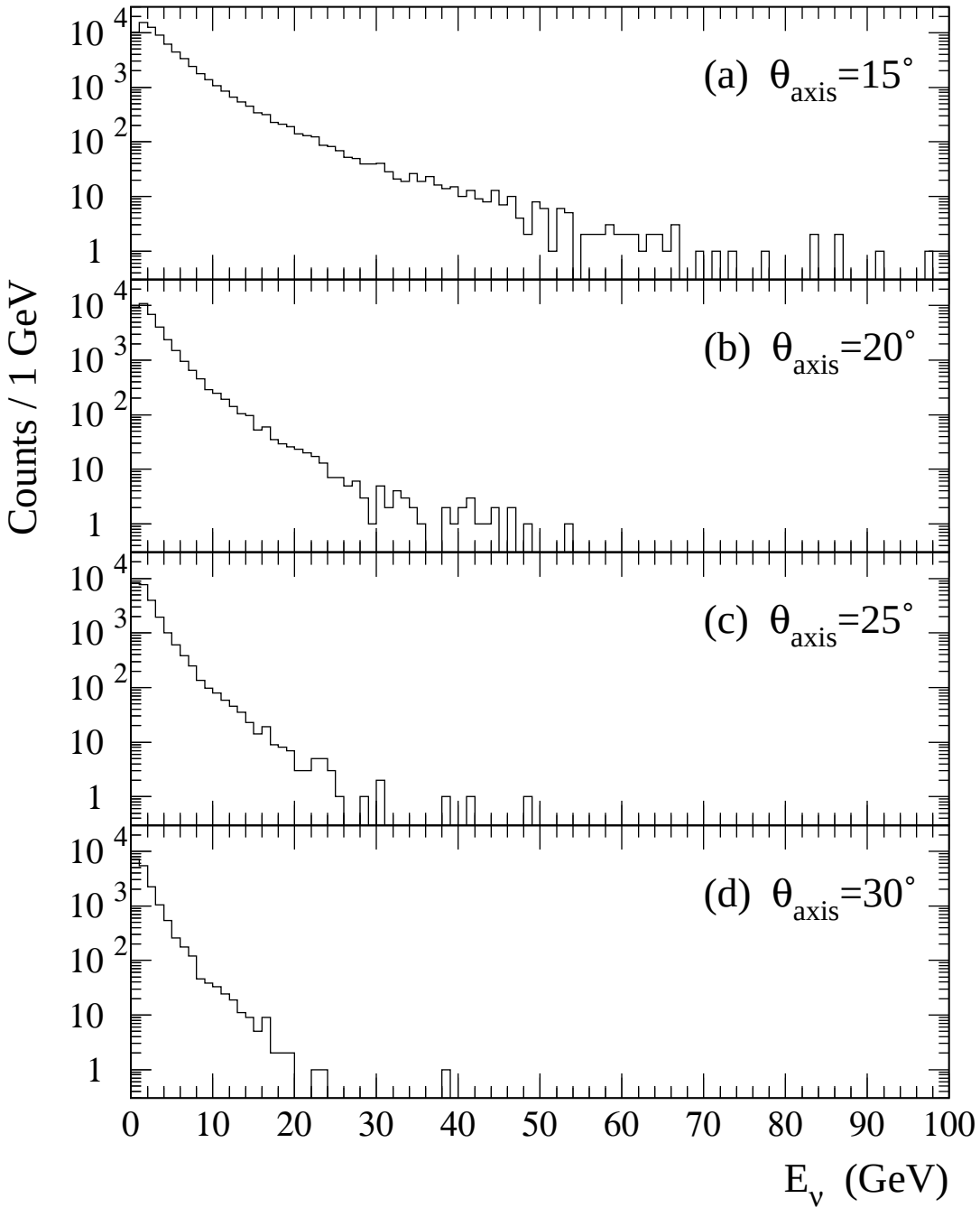

Figure 25: The energy spectra of the prompt neutrinos produced in the decay of bottom and charm hadrons for total 2.4×10^6 generated events. The polar angle of the tunnel axis $\theta_{\rm axis}$ is taken to be (a) 15°, (b) 20°, (c) 25°, and (d) 30°.

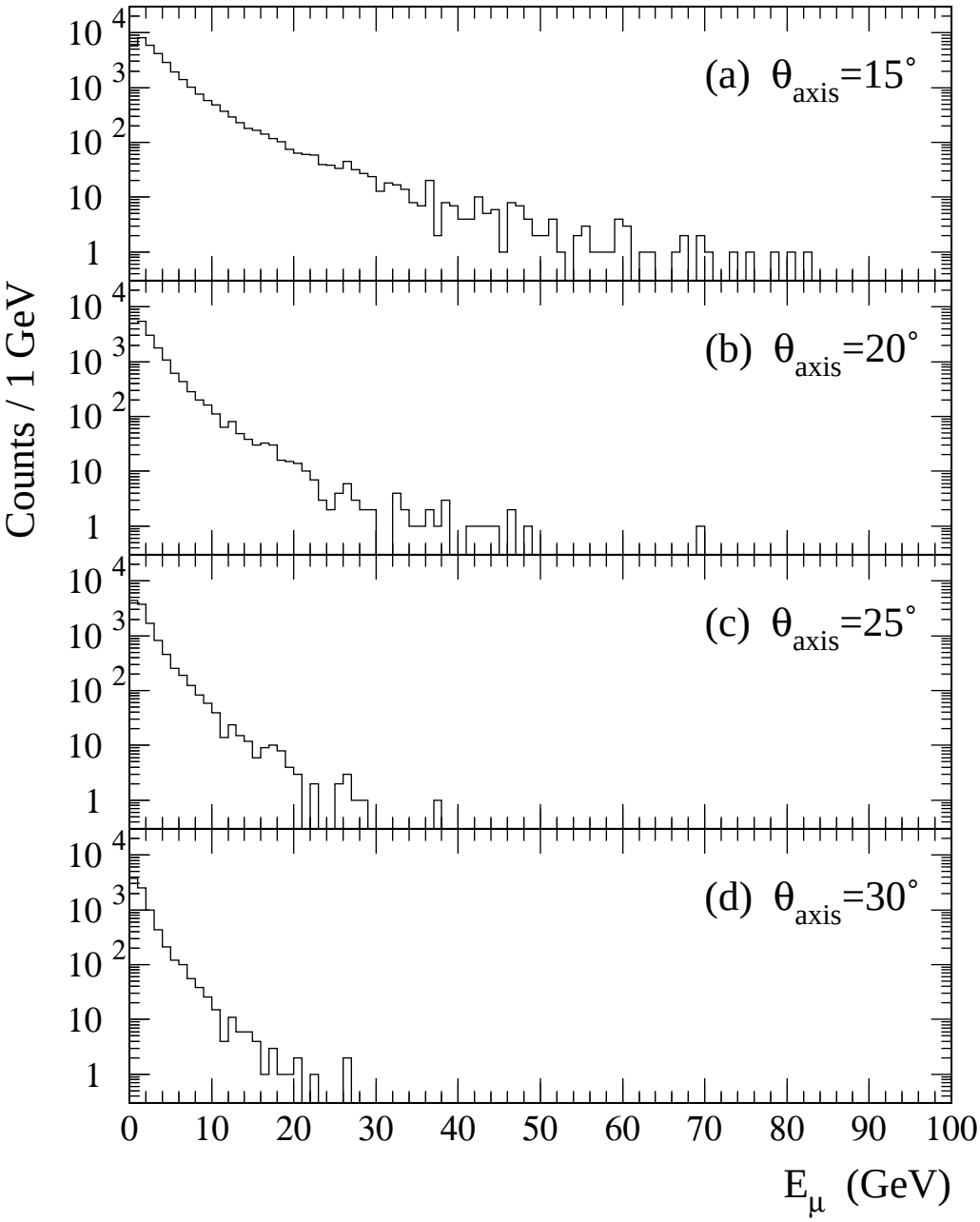

Figure 26: The energy spectra of the prompt muons produced in the decay of bottom and charm hadrons for total 2.4×10^6 generated events. The polar angle of the tunnel axis $\theta_{\rm axis}$ is taken to be (a) 15°, (b) 20°, (c) 25°, and (d) 30°.